BBA - Biomembranes 1867 (2025) 184452

Contents lists available at ScienceDirect

BBA - Biomembranes

journal homepage: www.elsevier.com/locate/bbamem

Research paper

Daptomycin membrane activity is modulated by the localized interplay between calcium ions and phospholipids in monolayers and bilayers containing a lysyl-phosphatidylglycerol analogue

Maria Hoernke [a,b], Shuai Shi [a], Alasdair T.M. Hubbard [c], Nina Geringer [d], Fabio Strati [e], Chen Shen [e], Christian Wölk [f,*], Richard D. Harvey [d,*]

[a] Department of Pharmaceutical Technology and Biopharmacy, University of Freiburg, Hermann-Herder-Strasse 9, 79104, Freiburg, Germany
[b] Department of Physical Chemistry, Martin-Luther-Universität, Von-Danckelmann-Platz 4, 06120, Halle (S.), Germany
[c] Department of Biosciences, School of Science and Technology, Nottingham Trent University, Nottingham, 15 NG11 8NS, UK
[d] Department of Pharmaceutical Sciences, University of Vienna, Josef-Holaubek-Platz 2, Vienna, Austria.
[e] Deutsches Elektronen-Synchrotron DESY, Notkestr. 85, 22607, Hamburg, Germany.
[f] Institute of Pharmacy, Medical Faculty, Leipzig University, Eilenburger Strasse 15a, 04317, Leipzig, Germany.

ARTICLE INFO

Keywords:
Daptomycin
Lysyl-phosphatidylglycerol
Phosphatidylglycerol
Staphylococcus aureus
Membrane perturbation
Membrane permeabilization/leakage
Antimicrobial resistance

ABSTRACT

Using the stable synthetic analogue 3-aza-dehydroxylysyl-phosphatidylglycerol (3adLPG), the putative role of native staphylococcal LPG in inhibiting the antibiotic daptomycin from binding to its target phosphatidylglycerol (PG), was investigated with respect to interfacial interactions between these lipids, daptomycin, and calcium ions. The influence of lipid monolayer/bilayer composition and interfacial ion concentrations upon the structure and integrity of model membranes were probed after daptomycin challenge using a combination of surface x-ray scattering techniques and fluorescence assays. In models representing the membrane composition of the daptomycin susceptible phenotype consisting of PG/3adLPG in a 7:3 M ratio, calcium ions drive the formation of two separate phases; Ca^{2+} cross-linked PG/PG pairs and PG/3adLPG ion pairs. Daptomycin is able to bind directly to the lipids in the PG/PG phase and increases the amount of interfacial Ca^{2+} ions to a level sufficient to displace 3adLPG from ion pairs with PG, and thus binds to its target PG. In bilayers with mixed chain lipids, daptomycin leads to pronounced membrane perturbations and enhanced permeability. Sequestering all of the available PG into PG/3adLPG ion pairs, therefore, would represent a putative daptomycin non-susceptible membrane. Daptomycin binding and the extent of subsequent lipid structural changes are reduced in these membranes. This implies that in bacteria, native LPG biosynthesis would need to ensure either an equivalence or an excess in relation to membrane PG content, in order for this mechanism alone to significantly contribute to daptomycin resistance.

1. Introduction

The bactericidal activity of the anionic lipopeptide antibiotic daptomycin has long been recognised as resulting from more than one membrane-associated mechanism of action [1]. At sub-micromolar concentrations (minimum inhibitory concentration - MIC 0.125–1.0 μg/mL or 0.08–0.6 μM), it is active against a narrow spectrum of Gram positive bacteria, including methicillin resistant strains of *Staphylococcus aureus* (MRSA) (MIC 0.5 μg/mL or 0.3 μM, minimum bactericidal concentration - MBC 2 μg/mL or 1.2 μM), which are in their logarithmic growth phase [1–4]. This low-concentration activity of daptomycin is achieved through the inhibition of peptidoglycan cell wall synthesis [5]. Higher daptomycin concentrations are required to produce an equivalent bactericidal effect against metabolically quiescent stationary phase *S. aureus* (MBC 32 μg/mL or 19.7 μM) in a manner which resembles the membrane permeabilising activity proposed for antimicrobial peptides (see SI figs. S1-S3) [1,6,7]. Although these two mechanisms are considered to be independent of each other, they both require the presence of calcium ions to facilitate bactericidal activity [8]. Daptomycin binds calcium ions to form complexes, the stoichiometric ratios of which have been described as ranging from 2:3 [9,10] to 1:2 [11]. Daptomycin-Ca^{2+} complexes are able to bind to anionic components of

* Corresponding authors.
E-mail addresses: christian.woelk@medizin.uni-leipzig.de (C. Wölk), richard.harvey@univie.ac.at (R.D. Harvey).

https://doi.org/10.1016/j.bbamem.2025.184452
Received 13 January 2025; Received in revised form 29 August 2025; Accepted 3 September 2025
Available online 8 September 2025

the bacterial cytoplasmic membrane. In addition to the requirement for calcium ions, the phospholipid composition of the plasma membrane also plays a pivotal role in both types of bactericidal activities of daptomycin. In particular, the proportion and location of phosphatidylglycerol (PG) within the membrane is important. In fact, PG, one of the lipids used in the current study (Fig. 1), has been recognised as a stereospecific target of daptomycin-Ca^{2+} complexes [5,11–17], with which it binds in a 1:1 stoichiometric ratio [14].

In actively dividing bacteria, daptomycin-Ca^{2+} targets regions of increased fluidity (RIF) in the plasma membrane [18]. The protein complexes responsible for cell-wall synthesis are localized in these RIF, [19] particularly in the division septum [5]. RIF are rich in lipid II, which facilitates the translocation of peptidoglycan building blocks from the cytoplasm to the cell wall region [18]. Through bridging calcium ions, oligomerised daptomycin forms complexes with lipid II and PG [5]. These membrane-located complexes effectively sequester the peptidoglycan monomers, thereby inhibiting cell wall synthesis [8]. Thus, the target and mechanism of daptomycin is similar to that of other antibiotics such as the glycopeptide vancomycin and the lantibiotic nisin, both of which, show significant cross-resistance with daptomycin [20–22].

In metabolically quiescent cells whose cell wall synthesis is suspended, daptomycin is thought to act in a PG-mediated membrane-targeted manner. It is proposed to permeabilize the plasma membrane, causing dissipation of ion gradients and cytoplasmic leakage. This mode of action requires a significantly higher concentration than the more specific activity of lipid II sequestration described above [1].

Since both of these mechanisms of action are reliant on the availability of PG in the *S. aureus* membrane to daptomycin-Ca^{2+}, mutations which facilitate the depletion of PG or an increase of other lipid species have been associated with resistance to daptomycin [23–26]. Specifically, mutations which lead to the dysregulation of the two phospholipid synthase genes, *mprF* and *cls* have been shown to lead to increased biosynthesis of lysyl-phosphatidylglycerol (LPG) and cardiolipin (CL) respectively, [24,25] both by consuming PG for their biosynthesis. Hence, it appears that one strategy of *S. aureus* resulting in daptomycin tolerance (in addition to teichoic acid neutralisation and cell wall thickening) [27] simply involves depletion of its target PG from the plasma membrane via conversion into other types of lipids [28]. In the majority of clinically relevant strains of *S. aureus*, in which the proportion of CL in the membrane is not significantly increased (at about 5–10 % total phospholipid content) [29], the most consistent findings has been that of increased LPG synthesis in daptomycin non-susceptible strains [23,27,30] facilitated by the MprF lysyl-transferase/flopase responsible for esterifying PG with lysine and translocating the newly-formed LPG (Fig. 1) to the outer leaflet of the plasma membrane [31]. When fully-ionised, cationic LPG is able to form discrete ion paired complexes with anionic PG [32]. Therefore, not only would LPG's increased biosynthesis deplete the membrane of PG as precursor in the biosynthesis, it would also potentially impair the remaining PG from interacting with daptomycin. This may partially explain why some daptomycin non-susceptible *S. aureus* strains exhibit a reduced affinity for cationic probes for membrane charge [23,30].

As mentioned above, the bivalent cation calcium is important for the interaction of negatively charged daptomycin with the likewise negatively charged PG lipids. Importantly, calcium ions are not only associated with daptomycin, but also with membranes in bacteria [33], having a strong affinity for both PG [34] and CL [35]. In the case of PG, calcium ions facilitate the formation of neutralised cross-linked complexes [36]. The proposed mechanisms of daptomycin are thus further complicated by the complex interplay between daptomycin, calcium ions, and LPG, all competing for electrostatic interaction with PG (and possibly also lipid II). This study applies biophysical techniques to shed light on the different lipid/lipid, lipid/calcium and daptomycin/lipid interactions at play, in order to investigate the role of PG/LPG ion pairs in daptomycin resistance.

Previous studies examining the role of LPG in daptomycin resistance have yielded somewhat inconclusive results. The, most important limitation for experiments is that LPG is inherently chemically labile. In LPG, the ester linking the lysine to the PG headgroup is readily hydrolysed under neutral and alkaline conditions [37,38]. This not only makes quantifying LPG in bacterial membranes using thin layer chromatography (TLC) with basic mobile phases [23,24,27,30,39,40] prone to underestimation [29], but it also complicates biophysical analysis using model systems due to relatively rapid degradation of the molecule whilst undergoing investigation [37]. Studies which have examined antimicrobial peptide association with liposomes containing mixtures of PG

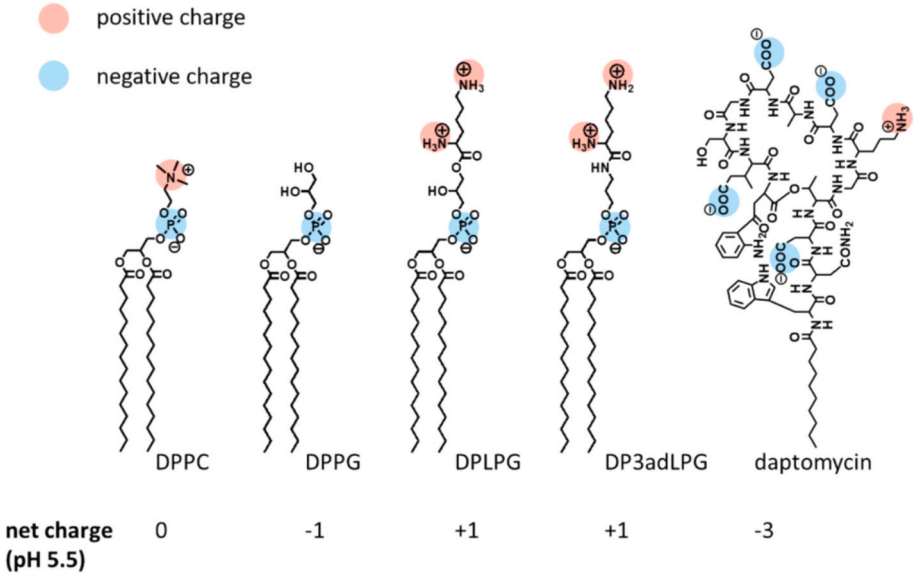

Fig. 1. Structures of the lipids associated with this study: dipalmitoylphosphatidylcholine (DPPC), dipalmitoylphosphatidylglycerol (DPPG), and dipalmitoyl-3-aza-dehydroxylysyl-phosphatidylglycerol (DP3adLPG), together with the structure of the lipopeptide daptomycin. The structure of lysyl-phosphatidylglycerol (DPLPG) is given for comparison with the headgroup of DP3adLPG. Although only the dipalmitoyl-derivatives of the phospholipids are shown, other alkyl chain versions were used in the studies as mentioned in the specific subsections. The given net charge at pH 5.5 is the dominating species of the molecule assuming pKa 10.5 for the δ- and ε-amines, pKa 7 for α-amines, pKa 2.6 for phosphate groups, and pKa 4.5 for carboxylic acid.

and synthetic native LPG have shown that in systems with PG/LPG ratios of 2.5 and above, the presence of LPG does not attenuate peptide binding [41–43]. In order to circumvent the problem of native LPG degradation, attention has turned to the use of stable LPG analogues such as lysyl-phosphatidylethanolamine (LPE) [44] and 3-aza-dehydroxylysyl-phosphatidylglycerol (3adLPG) [45] in biophysical investigations involving membrane active antimicrobials such as daptomycin.

Here, we aim to investigate the interplay of different types of lipids, calcium ions and daptomycin in molecular detail. In this study, we have used 3adLPG (Fig. 1) in biomimetic mixtures with PG in both lipid monolayer and bilayer model membrane systems in order to study the influence of interfacial calcium ions and ion paring between 3adLPG and PG on daptomycin-PG interactions. Experiments were conducted under mildly acidic conditions to mimic those encountered at the outer leaflet of the staphylococcal plasma membrane, due to the proton gradient present in living cells [46], and to encourage PG/3adLPG ion pair formation [45]. Two types of bacterial membranes were modelled, one representing daptomycin susceptible strains, based on lipid analysis which avoids the use of alkaline solvents, showing that the LPG content of wild type *S. aureus* and MRSA grown under mild conditions is approximately 30 % of the total phospholipids [29,47]. A membrane consisting of an equimolar PG/3adLPG mixture would thus represent a putative daptomycin non-susceptible *S. aureus* membrane. In using a monolayer model, we have been able not only to compare the daptomycin adsorption to a variety of lipid mixture interfaces, but also to measure changes in interfacial calcium concentration and correlate this with adsorption of daptomycin through monitoring changes in layer thickness and lipid packing geometries using a number of complementary x-ray techniques at the air/water interface. We have, thus, revealed a complex interplay of daptomycin with ions and charged lipids.

We have additionally measured the ability of daptomycin to induce membrane permeabilization in the presence of calcium ions for different lipid compositions in vesicles as a model bilayer system. In this context, the potential impact of lipid acyl chain saturation is examined by comparing membranes composed of POPG/POPC to those of POPG/DPPC. We chose these mixtures as enhanced daptomycin-induced membrane permeabilization has been observed in membranes where fully-saturated lipids are thought to form lateral domains within a matrix of fluid phase lipids [15].

In summary, we propose a complex picture of competing interactions of PG with LPG and daptomycin in the presence of calcium ions located at the membrane surface. These interactions influence the ability of daptomycin to not only bind to PG, but also to induce sufficient bilayer perturbation to cause membrane damage. We discuss the implications for both, the PG sequestering potential of LPG to shield against daptomycin interaction, and the membrane permeabilization caused by daptomycin when applied at higher concentrations.

2. Materials and methods

2.1. Materials

1,2-Dipalmitoyl-*sn*-glycero-3-phospho-(rac-1-glycerol) sodium salt (DPPG) and 1,2-Dipalmitoyl-*sn*-glycero-3-phosphocholine (DPPC), 1-palmitoyl-2-oleoyl-*sn*-3-phosphatidylcholine (POPC), and 1-palmitoyl-2-oleoyl-*sn*-glycero-3-phospho-(1′-racglycerol) sodium salt (POPG), were supplied by Avanti Polar Lipids (Alabaster, AL, USA). Dipalmitoyl-3-aza-dehydroxylysyl-phosphatidylglycerol (DP3adLPG) and 1-palmitoyl-2-oleoyl-3-aza-dehydroxylysyl-phosphatidylglycerol (PO3adLPG) were custom synthesised as described by Rehal et al. 2019 [45]. Daptomycin was supplied from SigmaAldrich. For the vesicle leakage experiments, 3-(N-Morpholino)-propane sulphonic acid (MOPS), NaCl, NaOH, HCl (all pro analysis grade) and chloroform (HPCL grade) were purchased from Carl Roth GmbH (Karlsruhe, Germany). Calcein (highest purity available) was obtained from Sigma-Aldrich (St. Louis, MO, U.S.A.).

All aqueous solutions were prepared using ultrapure water (resistivity above 18.2 MΩ.cm, Merck Millipore, Darmstadt, Germany).

2.2. The choice of model membranes and conditions

In previous work, we described a model system used to mimic the charge conditions of the *S. aureus* plasma membrane, using various binary mixtures of DPPG and DP3adLPG [48]. Under neutral environmental pH growth conditions, the common *S. aureus* lipid composition is similar to the PG/3adLPG [7:3] mixture [29], which we have used to represent the membrane composition of daptomycin susceptible strains. *S. aureus* strains can increase the amount of LPG when growing under acidic conditions, [29] represented by the PG/3adLPG [1:1] mixture, which we have used to model of daptomycin non-susceptible strains. In addition to the *S. aureus* relevant lipids, the PG/PC [7:3] mixture served as a control without ion pairing between the lipid species. The saturation pattern for the lipid acyl chains varied depending on the needs for the applied experimental methods and the scientific question which was addressed in those experiments. The details will be mentioned below in the relevant subsections.

The buffers and additives used were also selected to be appropriate for the different experimental techniques. Because of the requirement of calcium ions for daptomycin activity [11] and their relevance to natural bilayer structures due to their affinity for phosphatidylglycerol [34], most experiments were performed with a fixed amount of calcium at 1 mM $CaCl_2$, a concentration which does not limit the binding of daptomycin to membranes [9]. Furthermore, we wanted to be representative of the conditions encountered by daptomycin at its site of activity, i.e., mildly acidic pH present at the outer leaflet of the *S. aureus* plasma membrane [46] which would, therefore, also promote PG/LPG ion paring. Consequently, pH 5.5 was chosen for monolayer experiments and the fluorescence based daptomycin binding assay, a pH condition used in our previously published work on LPG [29,45]. The leakage experiments had to be performed at pH 6.5 (see details below), but mildly acidic conditions are also maintained at this pH value.

2.3. Monolayer experiments

For this set of experiments, monolayers were prepared exclusively with fully saturated dipalmitoyl chained lipids (DPPC, DPPG, and DP3adLPG), in order to highlight the effects of daptomycin on monolayer structures. In this context, stiff crystalline monolayer models are preferable to more fluid systems, as the rapid dynamics of the latter would allow lipid packing to rapidly reorganise within the timespan of the measurement (especially the long lasting GIXD scans), and we would lose the sensitivity for daptomycin-induced structural changes. The changes are initiated by daptomycin/lipid headgroup interactions at the monolayer/bulk interface and are readily detected via alterations in crystalline lipid packing, chain tilt, and size of crystallites. It should be noted that daptomycin itself is highly surface active (see SI fig. S4) and so any adsorption at the air/liquid interface in the presence of the lipid monolayers is likely to be enhanced by the surface activity.

2.3.1. Sample preparation for monolayer experiments

Lipids were used as 1 mM solutions in chloroform/methanol [8:2] for the preparation of Langmuir monolayers. DPPG, DPPC and DP3adLPG were premixed in chloroform/methanol to obtain the desired mixing ratios of the different binary mixtures. The corresponding solutions were spread onto the air/liquid interface and after solvent evaporation, the monolayers formed were laterally compressed to the desired lateral pressures π. As subphase, 1 mM $CaCl_2$ solution was used adjusted to pH 5.5 with HCl. For experiments in presence of daptomycin in the subphase, daptomycin was injected beneath a lipid monolayer which was compressed to 30 mN/m, using a Hamilton syringe, to yield a final concentration of 3 μM.

2.3.2. Setup for X-ray measurements at Langmuir monolayers

The GIXD, TXRF, and GIXOS experiments were performed sequentially on each sample, using the Langmuir grazing incidence diffraction setup [49] at the high-resolution diffraction beamline P08 (PETRA III, DESY, Hamburg, Germany) [50] at an incident energy of 15 keV (wavelength $\lambda = 0.827$ Å) and an incident angle of 0.07° (85 % of the critical angle of water). Binary lipid mixtures (DPPG/3adDPLPG [7:3] or [1:1] and DPPG/DPPC [7:3]) were deposited dropwise from solutions in chloroform/methanol [8:2] at the air/water interface (subphase: ultrapure water or 1 mM $CaCl_2$ solution pH 5.5) on a Langmuir trough (Riegler & Kirstein GmbH, Germany). The time-dependent effects of daptomycin adsorption on monolayer structure were monitored after daptomycin solution was injected (> 10 injection points) below the lipid monolayer, producing a final concentration in the trough of 3 μM (5 μg/mL). Final measurements were recorded after the systems had achieved steady state conditions (see SI fig. S5 and table S1).

For all of the x-ray measurements, the Langmuir trough was housed in a hermetically sealed container with Kapton windows transparent for x-rays, with the subphase maintained at a temperature of 25 ± 0.2 °C. The trough was constantly flushed with helium (He) to reduce the air scattering background and radiation-induced lipid damage (5 vol% air and 95 vol% helium). In order to reduce mechanically excited surface waves, a glass block was present in the subphase beneath the illuminated area of the monolayer.

2.3.3. Grazing incidence X-ray diffraction (GIXD)

Approximately 1 mm × 50 mm of the monolayer surface was illuminated. A vertically-mounted linear detector (Mythen2, Dectris, Baden, Switzerland) was rotated around the sample to detect the intensity of the diffracted beam as a function of the horizontal scattering angle 2θ, while the vertical pixel positions correspond to the vertical scattering angle α_f. A Soller collimator (JJ X-RAY, Denmark) was located between the sample and the detector to restrict the in-plane divergence of the diffracted beam to 0.08° full width at half maximum (FWHM). Model peaks taken as Lorentzian in the in-plane (Bragg peaks, Q_{xy}) and Gaussian in the out of-plane direction (Bragg rods, Q_z) were fitted to the integrated data using the peak fitting function within Origin version 2019 (OriginLab Corporation, Northampton, MA, USA). Thus, the Bragg peak positions and the centres of the Bragg rods were obtained which were subsequently used to determine the molecular areas, chain tilt angles, and lattice geometries of the monolayer condensed phases [51–55]. The Q_{xy} position of the equatorial Bragg peak maximum gives the intermolecular distance d ($Q = 2\pi/d$). The full-width at half maximum (FWHM) of the equatorial peak (instrument resolution-corrected by subtracting $Q_{xy} = 0.01$ Å^{-1}) [56] is used to calculate the size of the crystallite along the normal of the lattice line {hk} using the Scherrer equation ($L_{xy,hk} \approx 0.9(2\pi)/\mathrm{FWHM}_{corr}$ (Q_{xy}^{hk})), which gives an indication of size of the domains with crystal-like packing, or correlation length, in one dimension [57]. The dimensions of the unit cell, chain tilt angle (τ) with respect to the surface normal, and in-plane azimuthal orientation of the tilting (ψ^*) with respect to the lattice vector a' (see SI fig. S15) are given by $Q_z^{hk} = Q_{xy}^{hk}\, cos\psi_{hk}^*\, tan\tau$, [58] and were calculated with a custom-built fitting toolbox using Matlab (see SI table S3).

2.3.4. Total reflection x-ray fluorescence (TRXF)

Approximately 1 mm × 50 mm of the monolayer surface was illuminated by x-ray beam, and the fluorescence signal was detected by an Amptek X-100SDD detector (500 μm thick sensor, Amptek, Bedford, USA) placed almost parallel to the liquid surface and perpendicular to the photon beam axis at 12 cm from the X-ray footprint. This detector position was chosen in order to keep the Compton scattering at the given polarization of the photons as low as possible. The footprint centre of the incident beam was adjusted to the middle of the trough length along the beam direction, and at the middle of the view angle of the fluorescence detector [59]. The raw peak intensities were corrected to account for the attenuating effect on the evanescent wave intensity (I_e) of the subphase and the lipid monolayer, before subtraction of the background fluorescence intensity obtained with a lipid-free air/buffer interface (see SI figs. S7-S12). According to the equation $I_e = I_0 \bullet \exp.(-z/\wedge)$, the exponential decayed intensity I_e at the monolayer/subphase interface from the maximal measured evanescent wave intensity (I_0) at the air/monolayer interface is quantified by the monolayer thickness (z) and depth penetration decay length of the evanescent wave ($\wedge$) [60]. For these measurements, z was determined from the scattering length density profiles obtained from GIXOS data (Fig. 3) for the monolayers at each individual timepoint, and $\wedge$ is 90 Å at the chosen incident angle (85 % of the critical angle of air-water interface) [60]. The ratio of the concentration c_i of element i to the concentration c_P of phosphorous was calculated as $\frac{c_i}{c_P} = \frac{I_{x,i} \times \epsilon_{K,P}}{I_{K,P} \times \epsilon_{x,i}}$, where $I_{x,i}$ is the x-line emission intensity (x = K_α, K_β, L_α, …) of the element i after correction, $I_{K,P}$ is the K_α emission intensity of phosphorous. $\epsilon_{x,i}$ and $\epsilon_{K,P}$ are the detection efficiency of these emissions. It is calculated as $\epsilon_{x,i} = f_{SDD,E(x)} \times \sigma_{x,i}$, where $f_{SDD,E(x)}$ is the efficiency of the Amptek detector for the energy E of the x-line emission, being 75.5 %, 95.3 % and 87.8 % for the K_α of P, Ca and Cl, respectively. $\sigma_{x,i}$ is the cross section of the x-line emission of the element i under 15 keV incident beam, being 34.68, 263.27 and 85.31 b/atom for the aforementioned emissions, respectively [61]. The uncertainty of the method is given by the square root of the intensity of the element's X-ray emission, and the intensity uncertainties are propagated to the ratio (*absolute error* = $\frac{c_{element}}{c_P} \sqrt{\left(\frac{\sqrt{I_{element}}}{I_{element}}\right)^2 + \left(\frac{\sqrt{I_P}}{I_P}\right)^2}$). The transmission through the 12 cm path of 5 % air, 95 % helium is 100 % for the emission energies concerned, hence is not included in the evaluation.

2.3.5. Grazing incidence x-ray off-specular scattering (GIXOS)

GIXOS measurements used the same experimental set-up used for GIXD and TXRF with a narrower illumination area (0.25 mm × 50 mm). It permits the determination of changes in monolayer thickness and scattering length density [62,63] to be rapidly assessed in tandem with those of lipid packing geometry and interfacial ion concentration. Two vertical slits with 0.25 mm and 1 mm opening were placed behind the trough at 160 mm, and 653 mm from the pivot point. The off-specular scattering at 0.17° ($Q_{xy} = 0.04$ Å^{-1} at $\alpha_f = 0°$) was selected by horizontally offsetting both slits from specular plane [62]. The intensity profile as a function of Q_z was measured simultaneously using a Pilatus 100 k detector (Dectris, Baden, Switzerland) mounted 2 cm behind the 2nd slit.

The diffuse scattering intensity is measured as a function of Q_z at very small Q_{xy} ($Q_{xy} \approx 0$). This scattering intensity course $I(Q_z)$ (see SI fig. S16) is proportional to the product of the squared structure factor $|\Phi(Q_z)|^2$ of the monolayer and the Fresnel transmitivity $T_f(Q_z)$ from the air-water interface [63], where $\Phi(Q_z)$ is the Fourier transformation for the gradient of the scattering length density (SLD) profile perpendicular to the monolayer plane. T_f contributes to the Yoneda peak at the critical angle Q_c of the interface. Here, the Q_{xy} dependency of the capillary wave effect is neglected as it will only result in an apparently sharper interfaces [64,65], but not affect the thickness and density evaluation within the experimental accuracy. This approximation will not affect the validity of a qualitative evaluation on the trend of the change in roughness during the adsorption either.

2.4. Liposome experiments

For quantifying the binding of daptomycin to liposomes alone without examining structural changes in the lipid bilayers, we have selected model membranes predominantly in the fluid phase by using lipids with palmitoyl/oleoyl acyl chains. For a better link between the monolayer measurements and the dye leakage assay, daptomycin binding to liposomes containing PO3adLPG and those with DP3adLPG were compared.

The use of lipids with one or both saturated acyl chains for the dye leakage assays enables a comparison with previous studies examining the relative effects of LPG [41] and lipid chain saturation/unsaturation [15] on daptomycin-induced membrane permeabilization.

2.4.1. Daptomycin binding assays

The large unilamellar vesicles (LUVs) composed of various mixtures of POPC, POPG and PO3adLPG, were all produced from the re-solvation of dried lipid films to make a ~5 mM lipid dispersion in 20 mM HEPES buffered saline (pH 5.5, 150 mM NaCl). Each dispersion was extruded under compressed nitrogen pressure through 100 nm pore polycarbonate membranes (AMD Manufacturing Inc., ON Canada), for three passes using a LIPEX® Flow extruder (Evonik Inc., BC Canada) at 25 °C.

A 10:1 POPG/daptomycin molar ratio was achieved for each ternary lipid mixture liposome type, by adding equal volumes of a ~ 556 μM liposome dispersion to an 11 μM daptomycin solution. Following the method described by Moreira and Taylor [43], each column of an Invitrogen™ 96-well black-walled, clear-bottomed fluorescence microtitre plate was pre-prepared to contain 10 μL of $CaCl_2$ solution at eight different concentrations (ranging from 0.01 to 100 mM). For each liposome type, 90 μL of the liposome/daptomycin mixture was added to the wells in each column (in triplicate) to give a final volume of 100 μL containing ~250 μM lipid, ~5 μM daptomycin and $CaCl_2$ in a range from 0.001 to 10 mM. The same mass of POPC/POPG 4:1 was used for the binary control mixture, was also used in all of the ternary lipid mixtures which additionally contained PO3adLPG. All solutions were in 20 mM HEPES buffered saline.

The daptomycin binding assay is based on measuring the fluorescence of the kynurenine residue, the intensity of which is proportional to the degree of binding to lipid membranes [66]. Fluorescence intensity was recorded with an Infinite 200Pro fluorimeter (Tecan Group Ltd., Grödig, Austria) using an excitation wavelength of 360 nm (9 nm bandwidth) and an emission wavelength of 448 nm (bandwidth 20 nm) at 25 °C. Post measurement, background-corrected normalized I_{448} values were plotted against $CaCl_2$ concentration and fitted using the non-linear regression analysis tool in GraphPad Prism for macOS version 10.4.0 (GraphPad Software, MA, USA) with the four-parameter Hill function:

$$I_{448} = I_{min} + \frac{x^a \bullet (I_{max} - I_{min})}{x^a + {K_{0.5}}^a}$$

where I_{min} is the baseline fluorescence intensity, I_{max} is the maximum fluorescence intensity, a is the Hill coefficient, and $K_{0.5}$ is the half-saturation constant; the concentration of $CaCl_2$ required to achieve sufficient daptomycin/PG binding to elicit half of the maximum fluorescence intensity.

2.4.2. Fluorescence lifetime-based leakage assay

The leakage assay determines fluorescence lifetimes of calcein entrapped in large unilamellar vesicles as introduced in Patel et al. 2009 [67] and described in detail in Shi et al. 2022 [68]. Briefly, LUVs composed of different lipid mixtures (POPG/DP3adLPG [6:4], POPG/DP3adLPG [7:/3], or POPG/POPC [7:3]) were produced by hydration of dried lipid films with calcein buffer (70 mM calcein and 25 mM MOPS, pH 6.5 or pH 7.5), five free-thaw cycles, and extrusion (31 times) through 80 nm polycarbonate membranes (Nuclepore Track-Etched Membranes, Whatman International Ltd., Maidstone, UK) using a LiposoFast hand extruder (Avestin, Ottawa, Canada). The external calcein was removed on a PD-10 desalting column (GE Healthcare, Little Chalfont, UK) by eluting with isotonic MOPS buffer (130 mM NaCl and 25 mM MOPS, pH 6.5 or pH 7.5). Vesicle sizes were examined by dynamic light scattering on a Malvern Nano ZS (Worcestershire, UK) and lipid concentration was determined using Bartlett assay [69].

Daptomycin solutions were preincubated without/with $CaCl_2$ (0.3 mM or 1 mM in buffer) for 1 h before the leakage experiment. Calcein-loaded vesicles were injected into various concentrations of daptomycin to a final lipid concentration of 30 μM. Samples were incubated for the indicated times on a rocking MHR 13 Thermoshaker (400 U/min, Hettich Benelux, Geldermalsen, Netherlands) at 25 °C before measurement.

Time-resolved fluorescence decay curves were recorded at 515 nm using time-correlated single-photon counting (TCSPC) on a FluoTime 100 (PicoQuant, Berlin, Germany) with a 467 nm laser diode pulsed at 1 MHz for excitation. The biexponential fit of decay curves and determination of the total leakage (L_{total}) were performed as described previously [68].

3. Results

In order to better understand the influence of PG/3adLPG ion pairing on the effects of daptomycin on membrane barrier function, we first examined the nanoscale structural changes induced by daptomycin interaction with monolayer systems. This approach serves to correlate structural changes with the functional effects in bilayers which are putatively driven by them. The order in which the results are described follows this structure-function hypothesis.

3.1. Monolayer models

3.1.1. The charge state and interactions of lipid monolayers with ions: In equimolar PG/LPG mixtures, calcium is excluded from the lipid monolayers in absence of daptomycin

Total reflection x-ray fluorescence (TRXF) analysis was conducted on the lipid monolayers, concomitantly with x-ray scattering measurements, to study the presence of different ion species at the subphase-membrane interface and to evaluate the effect of ions on daptomycin interaction with the monolayer. With TRXF, detailed information about the ion composition of the electric double layer at Langmuir monolayer interfaces can be obtained within a depth of ~10 nm from the water surface (determined by the incident angle of the x-ray in this experiment) with an error of ≤10 % [70]. In common with the other grazing-incidence x-ray methods we used, the TRXF method is integrative and covers a specific area of the monolayer (50 mm × 1 mm), averaging emission from any potentially inhomogeneous distributions of daptomycin caused by the subphase injection method. It should be noted that TRXF is element and surface sensitive, e.g. quantified chlorine atoms in our experimental composition can only result from the chloride ions near the interface.

The relative quantities of detectible ions in proximity to the monolayer were determined by the integrated intensity of the characteristic K_α fluorescence emission peak of each element in the TRXF spectra obtained at different timepoints post subphase injection of daptomycin beneath the monolayers compressed to 30 mN/m (Fig. 2). The presence of three types of elements was examined; chlorine (Cl^- ions) and calcium (Ca^{2+} ions) from the subphase (K_α emission bands at 2.62 and 3.69 KeV, respectively), and phosphorous from the phosphate moiety of the lipids (K_α emission band at 2.05 keV) (for an example background corrected spectrum with indicated peaks see SI fig. S6).

The K_α emission intensity (I) normalized to the detection efficiency for the K_α directly reports on the excess concentration ratio between the Ca^{2+} and Cl^- ions and lipid headgroup phosphorous at the monolayer/buffer interface, to a depth of 90 Å. Hence, the Cl/P and Ca/P ratios were calculated for data interpretation. Here, we mainly consider the values after 20,000 s adsorption or longer.

Starting the evaluation of Cl at the monolayer/water interface, it appears that Cl^- ions remain mostly excluded from association with the lipid headgroups throughout the experiments. An exception is the daptomycin-free DPPG/DP3adLPG [1:1] monolayer, which has an Cl^-/P ratio of 0.02, indicating the presence of a small excess of positive headgroup charge, which allows electrostatic attraction of Cl^- ions. DP3adLPG can hypothetically attract Cl^- ions, since the lipid can be assumed to be fully ionised with a net charge of +1. Consequently, the

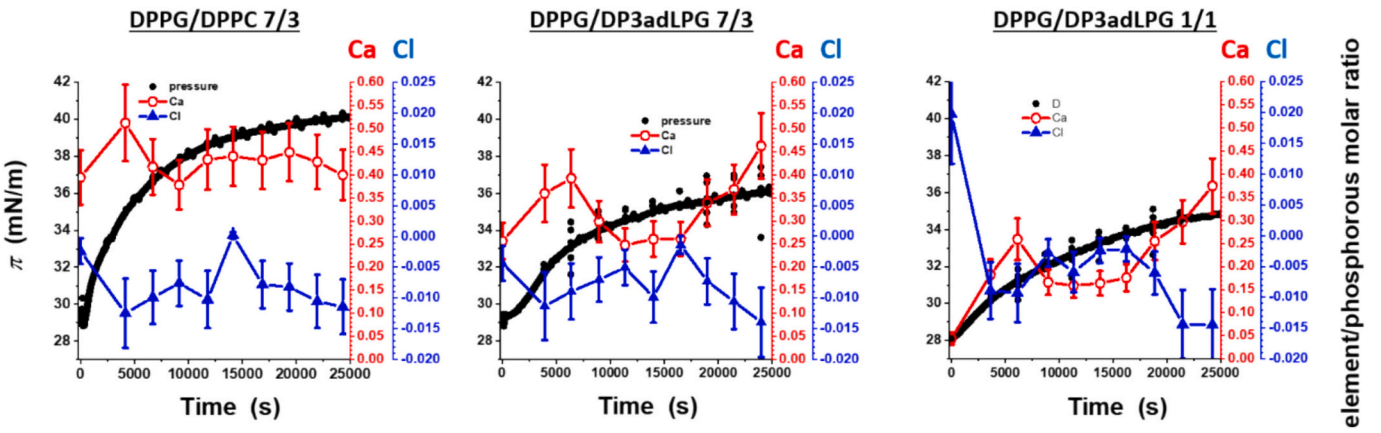

Fig. 2. The number of Ca (red circles) and Cl (blue triangles) associated with each phospholipid headgroup given as element/phosphorous ratio in the model monolayers, calculated from TRXF data, showing changes occurring during the daptomycin adsorption process. The monolayers consist of (A) DPPG/DPPC [7:3], (B) DPPG/DP3adLPG [7:3] and (C) DPPG/DP3adLPG [1:1]. The experiment started with monolayers compressed to ≈30 mN/m on a 1 mM $CaCl_2$ subphase at 25 °C. The timepoint of daptomycin injection (final subphase concentration ≈3 μM) was at $t = 0$ s, where the corresponding TRXF spectrum was taken before the injection. The daptomycin adsorption isotherm is given in black as a reference. If the adsorption isotherm starts below 30 mN, this was caused by a slight decrease of surface pressure during the subphase injection. The error bars represent the calculated error of the method given by √(element signal intensity). The TRXF spectra resulting in the calculated element/phosphorous ratios are presented in SI Figs. S7-S12. (For interpretation of the references to colour in this figure legend, the reader is referred to the web version of this article.)

theoretical Cl^-/P ratio could potentially be 0.5 in the DPPG/DP3adLPG [1:1] monolayer if one LPG attracts one Cl^-. Thus, the determined Cl^-/P ratio of 0.02 provides evidence for sequestration of the DP3adLPG headgroup amines by the formation of ion pairs with PG [48]. Interestingly, the Cl^- ions seem to be excluded from the DPPG/DPPC [7:3] and DPPG/DP3adLPG [7:3] monolayer interfaces (Fig. 2A and B), despite the relatively high initial amounts of Ca^{2+} ions associated with the lipid headgroups.

Evaluation of the interfacial calcium ion concentration allows a fuller interpretation of the changes occurring in the monolayers upon adsorption of daptomycin. First, we consider the various lipid monolayers without daptomycin in more detail. In the DPPG/DPPC [7:3] monolayer, the monolayer with the highest initial Ca/P ratio (0.39), the Ca^{2+} ions most likely form cross-links between lipid headgroup phosphates, potentially resulting in either PC/PC, PG/PG or PC/PG complexes. The depletion of Cl^- compared to the bulk concentration suggests that the interface is not entirely neutralised by Ca^{2+}, and anionic charge still persists. If all of the monolayer lipid headgroup phosphates were crosslinked by Ca^{2+} ions, the theoretical Ca/P ratio would be 0.5. The actual Ca/P ratio of the daptomycin-free system is closer to the scenario where Ca^{2+} ions were only able to cross-link adjacent DPPG molecules; a theoretical Ca/P ratio of 0.35. This is consistent with a previous finding, which showed that at bulk calcium concentrations below 50 mM, Ca^{2+} binds readily to PG, due to their electrostatic attraction [71].

The initial Ca/P ratio calculated for the daptomycin-free DPPG/DP3adLPG [7:3] monolayer, was 0.26. This is close to the value of 0.2, which would correspond to the theoretical Ca/P ratio from calcium cross-linked PG/PG complexes in coexistence with DPPG/DP3adLPG ion pairs, presenting a net neutral interface. The significant decrease in calcium binding to PG, compared with the PG/PC monolayer provides further evidence for the existence of DPPG/DP3adLPG ion pairs. The presence of a theoretically net neutral interface for the DPPG/DP3adLPG [1:1] monolayer (Fig. 2C) formed entirely from DPPG/DP3adLPG ion pairs is strongly supported by the negligible amount of Ca^{2+} ions detected.

Subphase injection of daptomycin changes the amount of headgroup associated ions. The effect is strongly dependent upon the lipid composition, despite the fact that the increase in surface pressure indicated that interfacial adsorption of daptomycin occurred with all three monolayers. The DPPG/DPPC [7:3] monolayer showed the largest overall increase in surface pressure. After an initial spike, the Ca/P ratio shows little deviation from the initial value, having an average of 0.43 ± 0.04 over the experimental time course. This may be due to the displacement of Ca^{2+} ions from PG/PG, in favour of the formation of Ca^{2+} bridged daptomycin/DPPG complexes. In summary, there is no overall change in interfacial calcium concentration. The DPPG/DP3adLPG [7:3] monolayer shows a biphasic increase in Ca/P ratio, which rises from 0.26 to 0.39 followed by a decrease and a final increase to 0.46 at the end of the considered timeframe. Excluding the last value, the Ca/P ratio is more fluctuating having an average of 0.31 ± 0.06, indicating a weak increase in Ca/P ratio by 0.13 compared to the absence of daptomycin. This could be due to either the displacement of PG from PG/3adLPG ion pairs, and subsequent association of PG with daptomycin via a Ca^{2+} bridge, or simply the accumulation of non-complexed daptomycin-Ca^{2+} at the interface, driven by its surface activity. A higher increase in Ca^{2+}/P ratio from 0.04 in absence of daptomycin to an average of 0.21 ± 0.08 is observed for the DPPG/DP3adLPG [1:1] monolayer, which might have occurred by the same two mechanisms but with a higher extent compared to the DPPG/DP3adLPG [7:3] monolayer.

3.1.2. Grazing-incidence X-ray diffraction (GIXD): daptomycin reduces lipid order only in PG/3adLPG [7:3] monolayers

Integration of the scattering intensities of the Bragg peaks observed in the GIXD diffractograms (see SI fig. S13), in both the Q_{xy} and Q_z directions, yields the peak centres from which the unit cell lattice parameters of alkyl chain packing can be calculated [57] (see SI table S2). Additionally, mean size of the crystallites in the plane of the monolayer (L_{xy}) in the liquid condensed phase was determined.

Prior to subphase injection of daptomycin, the DPPG/DPPC [7:3] monolayer exhibited a typical oblique unit cell geometry [54] (see SI fig. S15), indicated by the three distinct Bragg peaks visible in the diffractogram (see SI fig. S13). The average molecular area in the monolayer was 43.2 $Å^2$, the intermolecular spacing being 4.2 Å, with a chain tilt angle of 21° in the direction of the nearest neighbour (NN). The mean size of the crystallite along the plane normal of ~376 Å is indicative of highly ordered liquid crystals [72], the domains of which would contain an average of ~90 molecules in one dimension (L_{xy}/d). Similar to the DPPG/DPPC monolayer, the DPPG/DP3adLPG [7:3] mixture also exhibited an oblique unit cell geometry, with a molecular area of 43.8 $Å^2$, a chain tilt of 23° (NN direction), an intermolecular spacing of 4.2 Å

and a mean lateral size of the crystallite of ~400 Å (~96 molecules in one-dimension of the crystal). Only two distinct Bragg peaks were visible in the diffractogram of the DPPG/DP3adLPG [1:1] monolayer (see SI fig. S13), which is typical for an orthorhombic unit cell geometry [54] (see SI fig. S15). The unit cell of the equimolar mixture shows an area per molecule of 44.7 Å^2, a chain tilt angle of 26° (NN direction), an intermolecular spacing of 4.2 Å and a coherence length of ~450 Å (~108 molecules in one-dimension of the crystal).

After injection of daptomycin into the subphase, both, average molecular area, and chain tilt angle decrease concomitantly in all three of

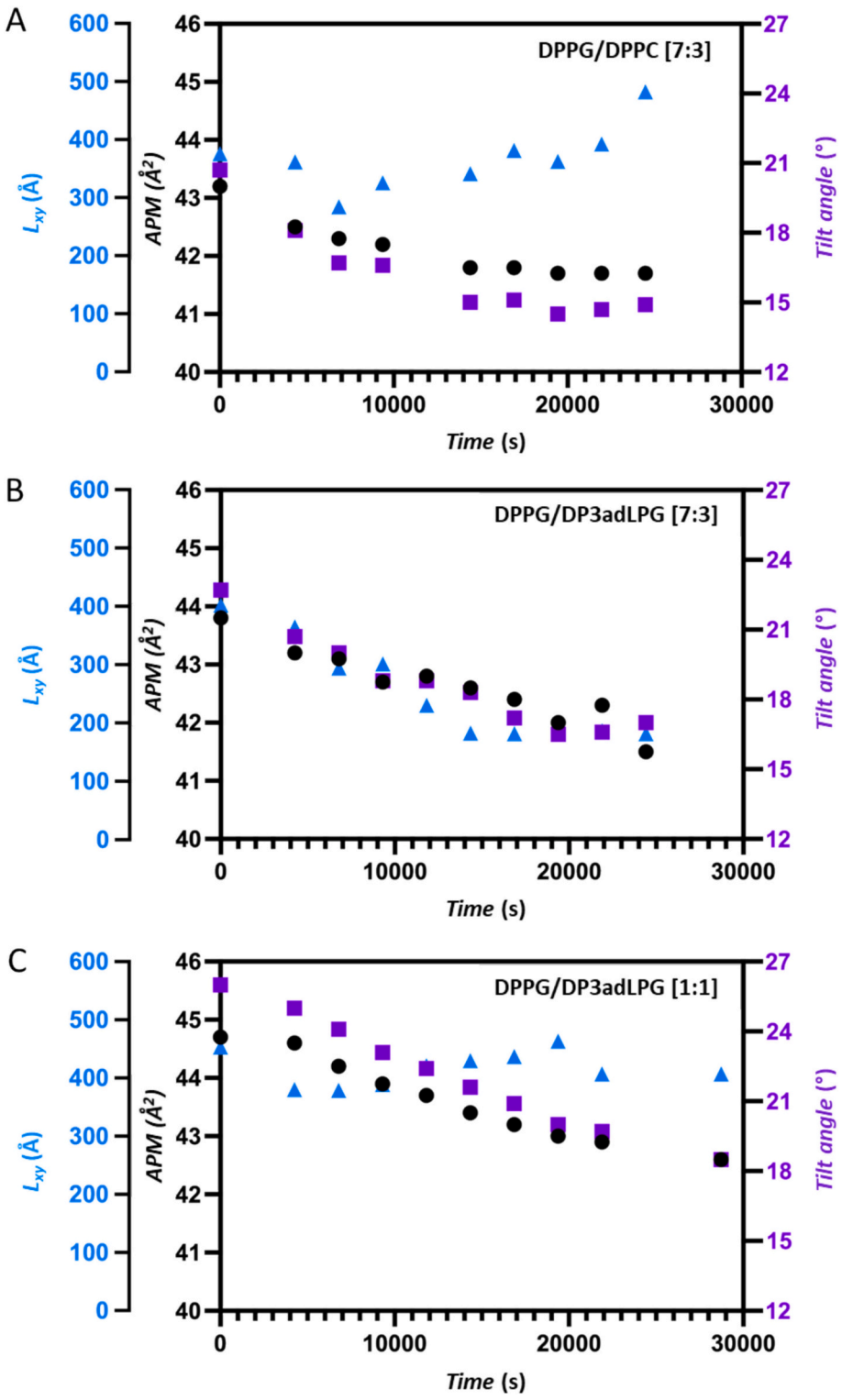

Fig. 3. Changes in average area per molecule (APM, black circles), chain tilt angle (purple squares), and mean size of the crystallite in the plane of the monolayer (L_{xy}. blue triangles) caused by the adsorption of subphase injected daptomycin (~3 μM) to monolayers of (A) DPPG/DPPC [7:3], (B) DPPG/DP3adLPG [7:3] or (C) DPPG/DP3adLPG [1:1], on a 1 mM $CaCl_2$ subphase at 25 °C, derived from the analysis of GIXD measurements. (For interpretation of the references to colour in this figure legend, the reader is referred to the web version of this article.)

the binary mixed monolayers (Fig. 3). This is likely caused by the adsorption of daptomycin to the air/liquid interface, instead of a specific interaction with the lipids. In consequence, the lipids in the monolayer are compressed. The smallest change in molecular area over the course of 8 h occurs in the DPPG/DPPC [7:3] monolayer (~1.5 Å^2). Both DPPG/DP3adLPG monolayers exhibit equivalent molecular area changes (~2.2 Å^2). The largest change in tilt angle was observed for the DPPG/DP3adLPG [1:1] monolayer (~7.6°), with the smallest change occurring in the DPPG/DP3adLPG [7:3] monolayer (~5.6°). In all three cases, however, the average intermolecular distance between the lipid molecules, remains 4.2 Å.

With respect to changes in mean size of the crystallite in response to adsorption of daptomycin (Fig. 3), the DPPG/DP3adLPG [7:3] monolayer shows a noticeably different trend compared to the other lipid mixtures. In both the DPPG/DPPC [7:3] and DPPG/DP3adLPG [1:1] monolayers, the correlation length fluctuates around a mean value instead of showing a clear increase or decrease over the course of the measurement. For the DPPG/DPPC mixture, the mean L_{xy} is 370 ± 50 Å averaged over the measurement time, whilst the DPPG/DP3adLPG [1:1] mixture shows less fluctuation in L_{xy} during adsorption (420 ± 30 Å). The L_{xy} of the DPPG/DP3adLPG [7:3] monolayer, on the other hand, decreases steadily over time from 400 to 180 Å, suggesting a clear reduction in domain size, which nevertheless still exhibit a high degree of long-range order. The greater change in domain size observed for the DPPG/DP3adLPG [7:3] monolayer also manifests as significant changes in Q_{xy} integrated peak intensities (see SI fig. S14).

Daptomycin therefore induces structural changes in all three lipid monolayers (decreasing both chain tilt and molecular area) to different extents. However, only for the DPPG/DP3adLPG [7:3] monolayer, a significant decrease of order (domain size of crystallites) was found, possibly induced by daptomycin disturbing the alkyl chain packing within the lipid crystallites of the monolayer in the liquid condensed LC phase state.

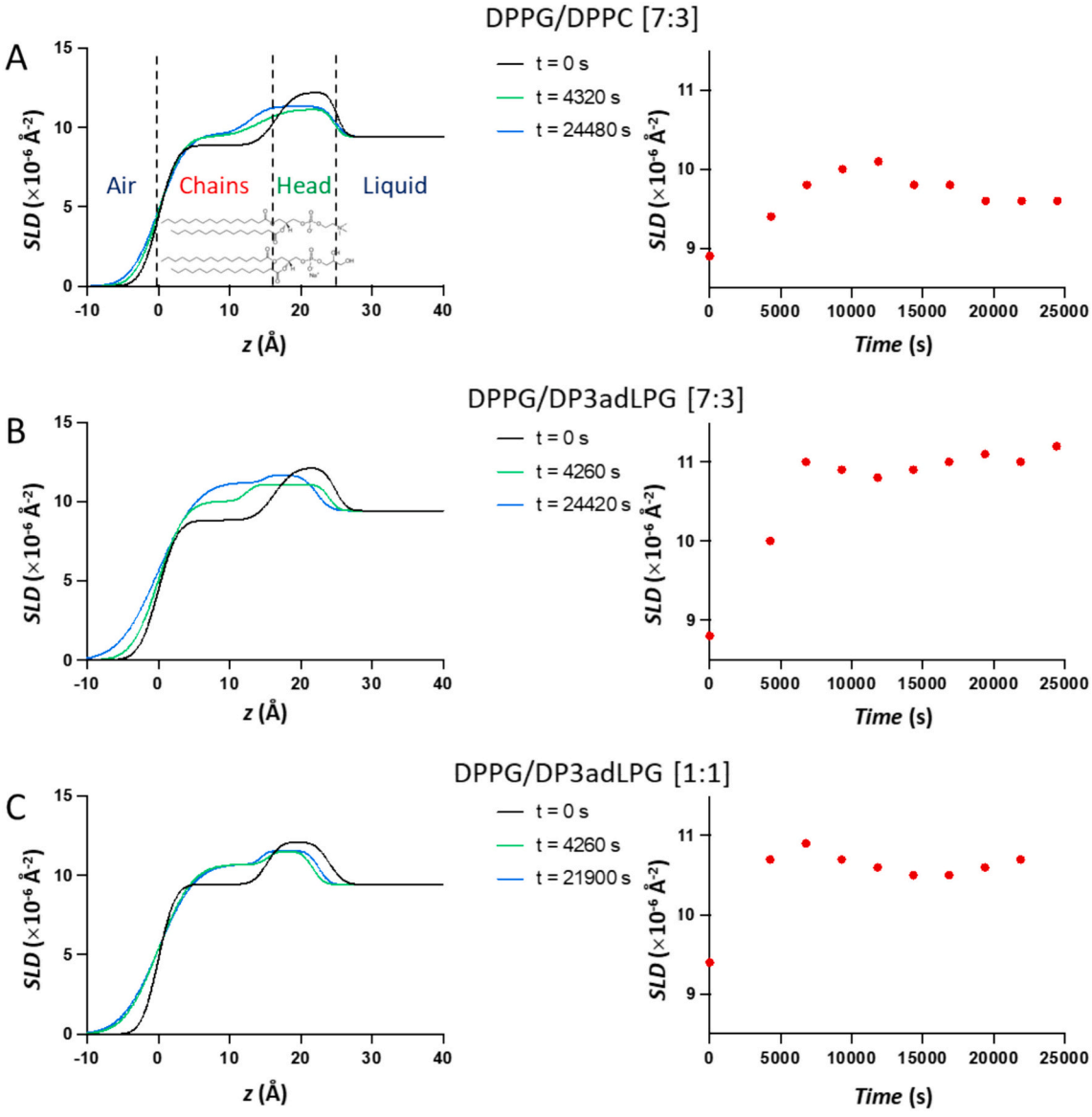

Fig. 4. X-ray SLD profiles derived from GIXOS intensity profiles (Q_{xy} = 0.04 Å^{-1}) fitted by a 2- compartment model, prior to subphase injection of daptomycin and at the first and final timepoints post injection (left panel). The changes in SLD of the compartment in contact with air assigned to the lipid acyl chains (without or with adsorbed daptomycin) over the complete experimental time course are plotted in the right panel. Monolayers are composed of DPPG/DPPC [7:3] (A), DPPG/DP3adLPG [7:3] (B) or DPPG/DP3adLPG [1:1] (C), at 25 °C.

3.1.3. Changes in monolayer thickness and density using GIXOS: PG/3adLPG ion pairing seems to reduce the daptomycin incorporation in lipid monolayers

Grazing incidence x-ray off-specular scattering (GIXOS) characterizes the scattering length density (SLD) profile of the surface layer normal to the surface plane providing structural information about orientation of lipids [62]. Here the SLD is related to the electron density of the moieties at different depths by the constant $r_e = 2.82 \times 10^{-5}$ Å, and hence represents the height and packing density of different regions of the lipid monolayer deposited at the air/liquid interface. In order to produce the monolayer density (SLD) profiles, the $I(Q_z)$ of a respective monolayer was fitted using a two-compartment model consisting of a headgroup compartment with SLD $\rho_{b,h,m}$ higher than the aqueous bulk $\rho_{water} = 9.43 \times 10^{-6}$ Å^{-2}, and a tail compartment with SLD $\rho_{b,t,m}$ lower than the headgroup region, performed with a custom-built fitting toolbox using Matlab. The interfaces of headgroup-bulk, tail-headgroup and air-tail were all modelled by error functions [73] and can be interpreted as roughness. The fitting of $I(Q_z)$ thus yields the thickness $D_{t,m}$, $D_{h,m}$ of the tail and the head compartment, their SLD and their roughness.

The SLD profiles (Fig. 4) encode information averaged over the entire area within the footprint of the x-ray beam (50 mm × 0,25 mm), covering also coexisting domains. In a pure phospholipid monolayer, the highest electron density is provided by the lipid headgroups, allowing a clearer distinction between the solvent water and the lipid acyl chains (illustrated in Fig. 4A). The roughness of the layers is illustrated by the slope of the SLD profiles at the junctions between the different layers. Zero roughness would be indicated by vertical junctions and a shallower slope represents a rougher interface. A high roughness might also indicate or be interpreted as an incompletely covered layer. Daptomycin has an overall higher SLD than the other components (calculated from the weighted sum of atomic scattering lengths to be ~11.45×10^{-6} Å^{-2}). Therefore, the increase in SLD of the tail and/or the headgroup region can be interpreted as daptomycin inserted between lipids located directly at the air-buffer interface. Whether the daptomycin is homogenously distributed or exists as lipopeptide clusters, cannot be distinguished due to the above-mentioned average signal.

For all three monolayers, the SLD profiles presented in Fig. 4 compare the monolayers before injection of daptomycin with those at ~4000 s (~1 h) and ~ 24,000 s (~7 h) after injection into the subphase. Additionally, the changes in SLD of the compartment in contact with air assigned to the lipid acyl chains are depicted over 21,000 s (~6 h) (left panels in Fig. 4). These indicate an increase of the SLD during daptomycin adsorption. In the case of the theoretically charge net-neutral DPPG/DP3adLPG [1:1] monolayer (Fig. 4C), the high surface activity of the daptomycin (see SI fig. S4) seems to drive the lipopeptide to adsorb at the air/liquid interface in spite of the presence of a lipid monolayer to which it has no net-electrostatic attraction. This occurs very rapidly and results in an increase in SLD of the compartment in contact with air assigned to the lipid acyl chains (by ~1.3×10^{-6} Å^{-2}). This indicates the presence of daptomycin, and a very slight thinning of both, the tail and headgroup regions caused by lipid splay. However, after the initial effect, the parameters describing the packing in the DPPG/DP3adLPG [1:1] monolayer remain relatively stable (see SI table S6), compared to the other lipid mixtures.

Daptomycin increases the SLD of the compartment assigned to the lipid acyl chains more in DPPG/DP3adLPG [7:3] than in DPPG/DPPC [7:3] monolayer (Fig. 4A). However, in the DPPG/DPPC [7:3] monolayer, the smaller density change is coupled with a more pronounced thinning of the tail layer and a thickening of headgroup layer (see SI table S4). This suggests that daptomycin interacts better with the anionic DPPG/DPPC or DPPG/DP3adLPG [7:3] monolayer than with a net-neutral DPPG/DP3adLPG [1:1]. We postulate that daptomycin incorporates somehow in the lipid monolayer inducing this structural change, e.g. thickening of the headgroup layer due to the large cyclic part of daptomycin. This supports the hypothesis that daptomycin is strongly attracted to PG-containing interfaces.

Although there are equivalent amounts of PG in the DPPG/DPPC [7:3] and DPPG/DP3adLPG [7:3] monolayers, the presence of ion pairing between the DPPG and DP3adLPG should theoretically reduce its anionic charge density, and in turn weaken its interaction with daptomycin. This is not observed, instead, the largest effect of daptomycin on the SLD of the compartment in contact with air assigned to the lipid acyl chains was observed for DPPG/DP3adLPG [7:3] (Fig. 4B). This may result from efficient penetration of daptomycin in the lipid monolayer. The tail thinning effect for the DPPG/DP3adLPG [7:3] mixture is not of the same magnitude as that observed for the DPPG/DPPC monolayer described above (see SI table S5).

3.2. Liposomal models

3.2.1. Daptomycin binding assays

The absence of any significant daptomycin binding to liposomes composed of either pure POPC, or the POPC/PO3adLPG mixture (Fig. 5) supports previous findings showing that the presence of PG is necessary to facilitate binding of daptomycin to membranes [5,12,13]. Although these assays were performed in order to determine the effect of 3adLPG on daptomycin binding to POPG, the incorporation of non-interacting POPC was necessary to maintain the colloidal stability of the liposomes containing equimolar quantities of POPG and PO3adLPG.

Fitting the daptomycin binding curves to the 4-parameter Hill function allows for comparison of the daptomycin affinities to the liposome formulations as a function of the increasing amount of calcium, with the restriction that we focus on the given 10:1 POPG/daptomycin molar ratio. As an indication of daptomycin/PG affinity, we calculated the $K_{0.5}$ value, the concentration of $CaCl_2$ required to achieve half the maximum daptomycin binding to the various liposome compositions with a fixed concentration of POPG (Table 1). The degree to which daptomycin binds to available POPG in the liposomes, is related to the increase in kynurenine fluorescence emission intensities above their baseline-corrected level (Fig. 5). Given that between the POPC/POPG 4:1 liposomes and any of those with ternary mixtures containing PO3adLPG, there is no statistically significant difference between the mean maximal fluorescence intensity achieved at saturation levels of daptomycin/POPG binding ($p > 0.05$ by Mann-Whitney U test) (Table 1), it may be assumed that similar degrees of binding were achieved for all of these liposomes. The influence of increasing the

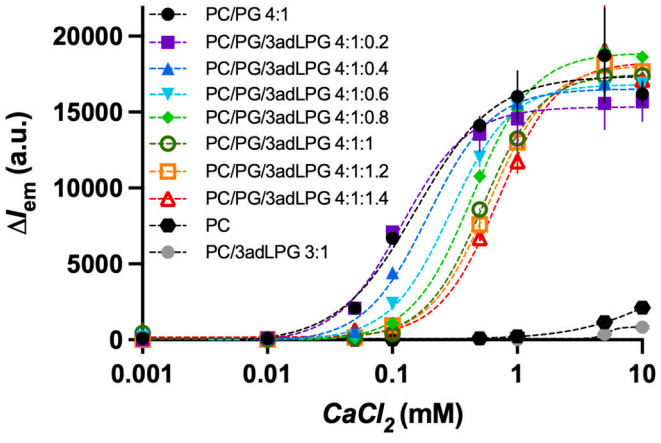

Fig. 5. Baseline-corrected kynurenine fluorescence emission intensity liposome binding curves for daptomycin, performed in 96-well microtitre plates. In line with the PC/PG 4:1 mixture, ternary lipid mixture wells contained ~278 μM of the PC/PG mix and all wells contained 5.5 μM daptomycin (10:1 POPG/daptomycin molar ratio), in 20 mM HEPES, 150 mM NaCl (pH 5.5) at 25 °C ($n = 3$). The dashed lines represent the curves obtained by fitting the mean binding data to a 4-parameter Hill function. The legend gives the molar ratios of the different lipid components.

Table 1
Parameters obtained from the Hill functions fitted to mean baseline-subtracted daptomycin binding curves obtained with various liposome formulations (10:1 POPG/antibiotic molar ratio) in 20 mM HEPES, 150 mM NaCl (pH 5.5) at 25 °C ($n = 3$).

Liposome composition	ΔI_{max} (a.u.)	$K_{0.5}$ (mM Ca^{2+})	a	R^2 of fit
POPC/POPG [4:1]	17,376 ± 1561	0.15 ± 0.02	1.4	0.969
POPC/POPG/PO3adLPG [4:1:0.2]	15,573 ± 636	0.13 ± 0.02	1.6	0.999
POPC/POPG/PO3adLPG [4:1:0.4]	16,533 ± 235	0.19 ± 0.004	1.7	0.997
POPC/POPG/PO3adLPG [4:1:0.6]	16,826 ± 854	0.29 ± 0.03	1.8	0.999
POPC/POPG/PO3adLPG [4:1:0.8]	18,916 ± 185	0.44 ± 0.03	1.9	0.999
POPC/POPG/PO3adLPG [4:1:1]	17,837 ± 108	0.53 ± 0.02	1.6	0.997
POPC/POPG/PO3adLPG [4:1:1.2]	18,095 ± 600	0.60 ± 0.05	1.8	0.999
POPC/POPG/PO3adLPG [4:1:1.4]	18,336 ± 1252	0.71 ± 0.04	1.8	0.994

proportion of PO3adLPG on the ability of daptomycin to bind to the POPG in the liposomes, could therefore be followed by observing the changes in the half-saturation ($K_{0.5}$). When the proportion of PO3adLPG was increased above 0.2, the mean $K_{0.5}$ of the POPC/POPG/PO3adLPG liposomes increased significantly compared to that of the POPC/POPG mixture ($p < 0.05$ by Mann-Whitney U test). In liposomes with 3adLPG proportions increasing from 0.4 to 1, a corresponding significant increase in mean $K_{0.5}$ was also observed ($p < 0.05$ by Mann-Whitney U test). This shows a clear effect of increased PG/3adLPG ion pairing in reducing daptomycin binding to POPG, which is independent of the degree of acyl chain saturation in 3adLPG (SI fig. S21 and table S8).

Increasing the content of PO3adLPG above parity with POPG, produces further correspondingly increases in mean $K_{0.5}$, of which only that observed between liposomes with 1.0 and 1.2 3adLPG proportions, is not statistically significant ($p > 0.05$ by Mann-Whitney U test). It is apparent from these data, that despite a (biologically questionable) large excess of 3adLPG, the daptomycin still shows significant POPG binding, suggesting that Ca^{2+} ions are able to make PG available to daptomycin by displacing 3adLPG from lipid ion pairs.

3.2.2. Membrane permeabilization

To characterize the membrane permeabilization induced by daptomycin, we performed vesicle leakage experiments. The daptomycin concentration, the lipid composition, buffer pH, and concentration of external calcium ions were all varied. Employing a well-established assay, a MOPS buffer and its matching calcein-containing buffer were used [68].

3.2.2.1. Stability of POPG/DP3adLPG vesicles upon addition of Ca^{2+}. Vesicles composed of POPG/DP3adLPG [7:3] were stable and did not leak entrapped calcein dye for at least 10 days in the absence of Ca^{2+} when stored at room temperature (data not shown). Furthermore, in the absence of daptomycin, no leakage was induced by Ca^{2+} up to at least 5 mM Ca^{2+} within 24 h (pH 6.5, SI fig. S17). However, increased particle sizes (caused by vesicle aggregation and/or fusion) were observed at 1 mM Ca^{2+} (SI table S7). To avoid this additional effect altering light scattering and potentially causing other side effects [68,74], leakage behaviour in various lipid compositions and pH conditions was evaluated with 0.3 mM Ca^{2+} only. Under these conditions, no indications of vesicle aggregation or fusion were observed in the absence of daptomycin.

For a better comparison to the monolayer model data, the fraction of DP3adLPG in the PG/LPG mixture was increased. However, vesicles composed of POPG/DP3adLPG [6:4] did not retain entrapped dye at pH 6.5 nor at pH 7.5 at room temperature. Even when prepared well above the gel-to-fluid melting point T_m (40 °C), the POPG/DP3adLPG [6:4] vesicles did not contain the dye even during preparation/purification of the vesicles. This indicates that a 6:4 mixture of POPG and DP3adLPG might suffer from packing defects. Preparing stable vesicles from POPG/DP3adLPG [1:1] was not possible due to colloidal instability probably caused by the net neutral charge. For evaluation of the membrane permeabilising effect, we focussed on the PG/LPG mixtures most relevant to *S. aureus*, as opposed to vesicles containing PC lipids that were used for understanding daptomycin binding (see Section 3.2.1).

3.2.2.2. Daptomycin induces leakage in POPG/DP3adLGP vesicles only in the presence of Ca^{2+}. Addition of at least up to 20 μM daptomycin to POPG/DP3adLPG [7:3] vesicles does not induce leakage for at least 5 h in the absence of Ca^{2+} (Fig. 6).

After preincubation with 0.3 mM or 1 mM Ca^{2+}, daptomycin induces leakage starting at ~1 μM reaching a plateau in the low μM range. With 0.3 mM Ca^{2+}, a maximum total leakage of approximately 30 % is reached after several hours. In the presence of 1 mM Ca^{2+}, probably higher leakage is reached, but the accuracy of this value might be compromised by changes in particle size. Thus, our data is consistent with the earlier observation that the extent of leakage increases with the calcium concentration [75]. Even though one might assume that at the lower concentration of 0.3 mM, the Ca^{2+} remains in excess compared to daptomycin, so that Ca^{2+} should not be a limiting factor for daptomycin activity [9], we cannot be entirely sure of that. The equilibria of daptomycin, Ca^{2+}, and diverse membranes warrant a study in its own right. The plateau in the leakage curve might indicate that the amount of daptomycin bound to the vesicles is not increasing further, even though the total concentration increases. Similar incomplete leakage has been observed in other cases [67,74,76,77].

It is likely that the calcium concentration determines the number of leakage events or the extent of leakage per individual leakage event. Most likely, Ca^{2+} limits the amount of daptomycin that is bound. Furthermore, leakage occurs rapidly and transiently, i.e., there is some leakage within 10 min of incubation, and the extent of leakage increases only slightly afterwards (SI figs. S18 and S19). To date, two options are considered: leakage arises from asymmetric-packing stress when the

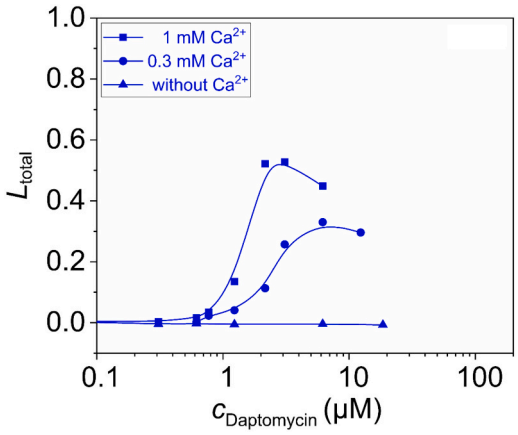

Fig. 6. Leakage induced by daptomycin in vesicles composed of POPG/DP3adLGP [7:3] in the absence and presence of Ca^{2+} (triangles: without Ca^{2+}; circles: with 0.3 mM Ca^{2+}; squares: with 1 mM Ca^{2+}) after 5 h of incubation. Solid lines are guides to the eye. (30 μM lipids, extruded LUVs of 130–140 nm diameter, pH 6.5, 25 °C. Daptomycin was preincubated with Ca^{2+} or buffer for 1 h. Entrapped buffer: 70 mM calcein, 25 mM MOPS; buffer outside: 25 mM MOPS, 130 mM NaCl).

amphiphiles insert into the outer membrane leaflet only, or leakage is related to membrane fusion [74,78–81]. Here, we cannot exclude a contribution of leakage caused by membrane fusion, however there are indications that make us consider this unlikely in the current case (see SI fig. S20 and text for more details).

3.2.2.3. The 3adLPG head group enhances membrane permeabilization. To investigate the influence of the 3adLPG head group on leakage, we compare to lipids with identical acyl chains, but zwitterionic PC head groups, i.e., POPG/DPPC [7:3] and POPG/DP3adLPG [7:3]. Daptomycin induces leakage in POPG/DPPC at much higher concentrations (starting at ~10 to 30 μM, red and orange data in Fig. 7) compared to POPG/DP3adLPG vesicles (~2 μM, blue data in Fig. 7). Leakage of POPG/DPPC membranes is also incomplete and also transient (SI figs. S18 and S19) suggesting that the mechanism of leakage is identical. Daptomycin has been shown to oligomerize on PG/PC membranes [82] which is often a preliminary stage of pore formation. Since daptomycin is expected to bind only to the POPG in either PG/PC mixture, it seems likely that daptomycin also oligomerises on both types of vesicle membranes. Therefore, the most likely explanation for the differences in membrane permeabilization caused by exchanging DPPC for POPC, is that the structural changes which occur in the membrane upon daptomycin binding are different. Potentially, more fluid POPG/POPC membranes are better able to self-heal defects when exposed to low concentrations of daptomycin. We cannot exclude an effect of different binding equilibria with the differing lipid compositions.

3.2.2.4. Daptomycin-induced leakage is facilitated in vesicles composed of saturated and unsaturated lipids. We examined the effect of differing lipid chains by comparing a mixture containing lipids with combined saturated and unsaturated chains (POPG/POPC) to a mixture containing both PO- as well as saturated-only DP-lipids (with POPG/DP3adLPG or POPG/DPPC head groups, respectively). Daptomycin is most active in vesicles containing lipids with mixed unsaturated and saturated chains (POPG/DPPC), with an additional effect of 3adLPG head groups (filled symbols in Fig. 7). With the same lipid head groups (PG/PC), vesicles are much less susceptible to leakage when all lipids contain unsaturated acyl chains (POPG/POPC) (squares in Fig. 7). This and similar work [15] indicate that potential packing defects between the lipid chains might facilitate leakage. We are aware that such packing defects are more likely in defined, binary model lipid membranes compared to full, biological membranes. Nevertheless, the larger LPG head group in conjunction with ion pairing with PG lipids might result in a tendency for non-lamellar phases [83], i.e., suboptimal lipid chain packing.

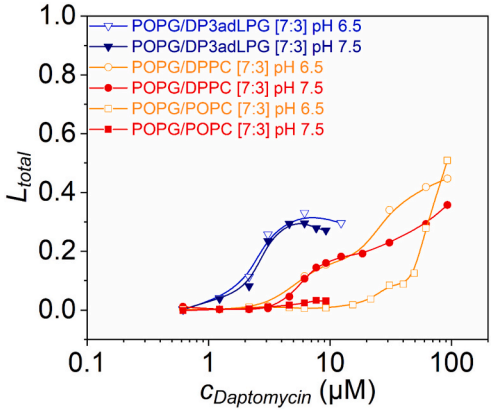

Fig. 7. Leakage induced by daptomycin in LUVs composed of POPG/DP3adLPG [7:3] (filled, blue: at pH 6.5; dark blue: at pH 7.5), POPG/DPPC [7:3] (filled, orange: at pH 6.5; red: at pH 7.5); and POPG/POPC [7:3] (open, orange: at pH 6.5; red: at pH 7.5). Solid lines are guides to the eye. (30 μM lipids, extruded LUVs of 110–140 nm diameter, 25 °C. Daptomycin was preincubated with 0.3 mM Ca^{2+} for 1 h. Entrapped buffer: 70 mM calcein, 25 mM MOPS; buffer outside: 25 mM MOPS, 130 mM NaCl). (For interpretation of the references to colour in this figure legend, the reader is referred to the web version of this article.)

4. Discussion

4.1. Could PG/LPG ion pairs play a role in daptomycin-Ca^{2+} resistance?

In staphylococci, daptomycin can act as both by inhibiting cell wall synthesis [5] at low concentration, and by permeabilizing membranes at high concentration (see SI figs. S1-S3). What these apparently separate mechanisms have in common is mediation via daptomycin specificity for the plasma membrane lipid phosphatidylglycerol, with which it forms a stereospecific 1:1 complex in the presence of Ca^{2+} ions [14,16]. For inhibition of cell wall synthesis, binding of daptomycin-Ca^{2+} complexes to PG stabilises a ternary complex with lipid II, inhibiting this precursor to the cell wall cross-linkages from advancing peptidoglycan biosynthesis [5]. The membrane permeabilizing activity of the daptomycin-Ca^{2+} complex is more directly mediated through its binding to PG. Membrane permeability is enhanced in PG-containing model membranes where daptomycin-driven demixing of fully-saturated and partially-unsaturated lipids is thought to facilitate the formation of domains coupled across both membrane leaflets [15]. Therefore a reduction in the proportion of PG in the bacterial membrane, through increased conversion to either lysyl-PG or cardiolipin [24,25], could be considered to provide some degree of resistance to both mechanisms of daptomycin-Ca^{2+} activity. Additionally, the increased biosynthesis of lysyl-PG may contribute to daptomycin non-susceptibility [84,85] by the sequestration of membrane PG into PG/LPG ion pairs [86]. Here, we study this putative role of PG/LPG ion pairing in daptomycin-Ca^{2+} resistance using our chemically stable substitute for native staphylococcal lysyl-phosphatidylglycerol DP3adLPG.

4.2. Defects in membrane lipid chain packing enhance daptomycin-Ca^{2+}-induced membrane perturbation

The liposome leakage studies presented here show that the presence of non-target PC lipids with fully-saturated chains facilitate membrane leakage from POPG/DPPC [7:3] liposomes exposed to daptomycin. This is in marked contrast to POPG/POPC liposomes which showed negligible leakage when challenged with daptomycin concentrations below 10 μM, but which would be expected to elicit substantial binding of daptomycin. Mixing fully and partially saturated chained lipids has previously been shown to enhance daptomycin-induced membrane leakage in liposomes containing fully saturated DSPG [15]. Clearly the presence of non-target fully-saturated lipids such as DPPC leads to similar effects. Substituting DPPC with DP3adLPG in the PG/3adLPG [7:3] daptomycin-susceptible membrane model resulted in an even more pronounced membrane leakage, despite the putative protective role of PG/3adLPG ion pairing. Although previous studies have shown that the presence of native LPG in fluid phase liposomes does not inhibit daptomycin binding [42,43], it has not been reported how this might influence membrane permeability. Although the degree of daptomycin binding was independent of 3adLPG chain saturation (SI fig. S21 and table S8), the influence of non-target lipid chain saturation is a possible contributing factor in leakage enhancement, as in the example of the POPG/DPPC mixtures. Daptomycin was clearly able to bind to the PG in the POPG/DP3adLPG [7:3] liposomes, either through displacing the Ca^{2+} ions that cross-link adjacent fluid phase PG headgroups [87,88], and/or by displacing the cationic lipid from PG/3adLPG ion pairs. The propensity for equimolar DPPG/DP3adLPG ion pairs to form inverse hexagonal (H_{II}) phases [83], most likely through splaying of the lipid tails, may be enhanced by the oleoyl chain in POPG. This, in turn, facilitates the observed enhanced dye leakage. The use of POPG/DP3adLPG [7:3] liposomes as model daptomycin-susceptible strain

membranes supports the ability of daptomycin to bind and permeabilize these types of membranes. However, it remains unclear from the leakage data what role if any, is played by LPG in daptomycin tolerance [31]. This points to a more important role for the calcium ions present at the interface in facilitating daptomycin/PG interactions, especially in the presence of LPG head groups.

4.3. Ca^{2+}-induced lateral demixing in mixed lipid monolayers enhances daptomycin adsorption

The apparent discrepancy between the rapid and high degree of interfacial adsorption of daptomycin-Ca^{2+} to the DPPG/DPPC monolayer (see SI fig. S5) or its high affinity for POPC/POPG liposomes (Fig. 5) and the comparatively low membrane permeability of POPG/POPC vesicles, provides a useful illustration of the extent to which daptomycin-induced membrane permeabilization is dependent upon both lipid chains and headgroups [15]. The TRXF experiments indicate the presence of relatively high amounts of Ca^{2+} at the interface of the DPPG/DPPC [7:3] monolayer, which most likely cross-link DPPG headgroups to form neutral dimers which mix well with the zwitterionic DPPC. Evidence for the monolayer DPPC itself having little or no interaction with Ca^{2+} to form cationic pairs comes from the relative scarcity of Cl^- counter ions within the interfacial region. In this situation, PG might be considered to be shielded from interactions with daptomycin-Ca^{2+}. However, this seems not to be the case as daptomycin clearly adsorbs to DPPG/DPPC [7:3] monolayers causing changes in lipid packing (GIXD data) and monolayer density (GIXOS data). Daptomycin-Ca^{2+} likely displaces the Ca^{2+} from the salt-bridged PG dimers to strongly bind to the lipid, aided by the binding pockets in its cyclic peptide moiety which have a strong affinity for the hydroxyl groups of the PG headgroup glycerol [14].

Adsorbed daptomycin takes up space at the air/liquid interface and thus condenses the lipids, decreasing the average molecular area and chain tilt angle (schematic illustration Fig. 8). Because daptomycin does not form a well-defined and tightly packed layer, adsorption also increases the interfacial roughness determined in GIXOS experiments. The consistency of the lateral size of crystallites in the LC phase of the lipids, even upon adsorption of daptomycin, implies that some daptomycin adsorbs; most likely in the non-crystalline part or at the edges of crystallites. Another part of the bound daptomycin probably oligomerises and faces the subphase. Oligomerisation of daptomycin-Ca^{2+} bound to PG may also facilitate the lateral sequestration of PG from non-interacting PC both, in monolayers (schematic illustration Fig. 8) and vesicle bilayers. This might possibly facilitate packing defects in the mixed chain POPG/DPPC [7:3] vesicles, leading to a significant increase in dye leakage compared to POPG/POPC [7:3] vesicles [15]. Whether this effect of lipid chains is relevant beyond binary mixed model membranes to biological membranes remains doubtful due to the more fluid nature of the latter, but it can help us to understand how daptomycin-Ca^{2+}/PG interactions have a propensity to alter the structures of mixed lipid systems.

4.4. Demixing in PG/3adLPG systems may enhance their perturbation by daptomycin-Ca^{2+}

For assessing the influence of lipid headgroup ion pairing on daptomycin/lipid interactions, PC was substituted with the LPG analogue 3adLPG in both monolayer and bilayer models. For the biomimetic daptomycin-susceptible PG/3adLPG ratio [7:3] [29], the type and extent of interaction with daptomycin-Ca^{2+} was different to that observed with DPPG/DPPC 7:3 monolayers. In the absence of Ca^{2+} ions, DPPG/DP3adLPG [7:3] monolayers have a significant anionic charge [48]. The relatively high amount of Ca^{2+} ions detected in the interfacial region of the PG/3adLPG [7:3] monolayer suggests that calcium interacts with excess PG in the lipid mixture resulting in an effectively neutralised monolayer consisting of DPPG/DP3adLPG ion pairs and calcium-bridged PG dimers, as suggested by the TRXF data (Fig. 2 and schematic illustration Fig. 8). Addition of daptomycin-Ca^{2+} increases the surface pressure and interfacial roughness, and decreases the average molecular area and lipid chain tilt. This may be attributed to two effects: firstly, the displacement of Ca^{2+} ions cross-linking dimerised PG molecules to form daptomycin-Ca^{2+}-complexed DPPG, and secondly the adsorption of daptomycin-Ca^{2+} directly at the air/liquid interface, both of which would serve to increase the lipid packing density. Subsequently, increased interfacial calcium may also make the PG/3adLPG [7:3] model membranes sensitive to daptomycin by displacing the cationic lipid from PG/3adLPG ion pairs and binding to its target PG (schematic illustration Fig. 8). This is also evident from the liposomal binding experiments, which show that calcium is able to displace 3adLPG from ion pairs with PG. In contrast with the DPPG/DPPC [7:3] monolayer, the mean size of crystallites of the PG/3adLPG [7:3] monolayer significantly decreases upon interaction with daptomycin.

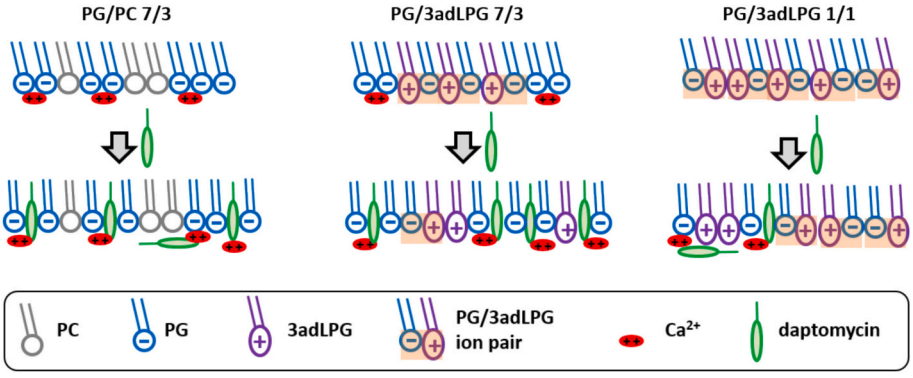

Fig. 8. The putative effects of daptomycin in presence of Ca^{2+} on various binary lipid mixtures. The effects are shown at the lipid monolayers at the air/liquid interface, prior and subsequent to subphase injection of daptomycin, but also can be postulated for lipid bilayers. In PG/PC 7:3 monolayers, daptomycin-Ca^{2+} binds to DPPG by displacing the Ca^{2+} which cross-links adjacent anionic headgroups. This facilitates interfacial adsorption and insertion of daptomycin. In presence of 3adLPG in the PG/3adLPG [7:3] mixture, the lipid mixture becomes more sensitive to daptomycin. Daptomycin efficiently incorporates in the lipid mixture and vesicles become more permeable. The interaction of the lipid mixture with daptomycin-Ca^{2+} can induce the release of PG from ion pairs. In the PG/3adLPG [1:1] mixture, the lipid ion pairing dominates the electrostatics at the lipid/subphase interface resulting in a strong reduction in calcium binding. Also, the interaction with daptomycin is reduced. Even if a certain adsorption was detected, the incorporation of daptomycin seems to be reduced. The acyl chain of daptomycin will most likely be shielded from water even if daptomycin is not inserted into the membrane potentially by oligomerization, not illustrated. The schematic illustration is a summary the main hypotheses resulting from our findings, aspects of binding geometry, stoichiometry or direct binding partners are not intended to be accurately represented.

This is probably due to enhanced lateral separation of the DPPG/DP3adLPG ion pairs from patches enriched in DPPG with bound daptomycin. In the POPG/DP3adLPG [7:3] vesicles, this putative lateral separation may be further enhanced by unfavourable packing of POPG with mixed acyl chains and DP3adLPG with saturated acyl chains. This presumed enhanced lateral separation would likely further promote membrane perturbation compared to those composed of POPG/DPPC as observed in our leakage experiments. The fraction of DPPG involved in ion pairs with DP3adLPG in the investigated DPPG/DP3adLPG [7/3] monolayers in the presence of Ca^{2+} could not be determined with our experiments. However, the monolayer adsorption data which shows a lower final surface pressure suggests that there is less daptomycin-Ca^{2+} adsorbed to the DPPG/DP3adLPG [7:3] monolayer compared to DPPG/DPPC [7:3] (see SI fig. S5). The liposomal binding assays support this, in showing that daptomycin affinity is slightly reduced in the presence of 3adLPG. This is actually in accordance with what is expected assuming less electrostatic attraction of daptomycin-Ca^{2+} to the less negatively charged PG/LPG compared to PG/PC. Nevertheless, according to the reduced size of crystallites and the increased interfacial roughness in DPPG/DP3adLPG [7:3] compared to DPPG/DPPC [7:3], the daptomycin induces more pronounced structural changes in the presence of 3adLPG, a fact which also supports the more significant dye leakage observed in the DPPG/DP3adLPG [7:3] liposomes.

4.5. PG/3adLPG ion pairing does provide some protection against daptomycin-Ca^{2+} binding

A significant advantage of using the monolayer model is that it allows the study of daptomycin interactions with net-neutral PG/3adLPG [1:1] mixtures, which is not possible in liposome dispersions without the presence of high amounts of PC, due to colloidal instability. In the absence of daptomycin, the DPPG/DP3adLPG [1:1] monolayer attracts Cl^- ions, indicative of a slightly positive interfacial charge. This may indicate the presence of a small portion of Ca^{2+} bridges between adjacent PG molecules instead of a layer formed entirely of PG/3adLPG ion pairs, in which non-paired 3adLPG could attract chloride ions. Overall, the monolayer would still predominantly consist of DPPG/DP3adLPG ion pairs (schematic illustration Fig. 8) [48]. After subphase injection of daptomycin, the PG/3adLPG ion pairs seem to be disrupted to a small extent, possibly by a competing daptomycin-Ca^{2+}/DPPG interaction. Calcium ion concentration certainly increases at the interface upon adsorption of daptomycin. This increase results in smaller amounts of Ca^{2+} ions at the interface of DPPG/DP3adLPG [1:1] monolayers compared to DPPG/DP3adLPG [7:3] or DPPG/DPPC [7:3]. Displacement of 3adLPG from PG/LPG ion pairs, which can be assumed by daptomycin binding in the liposomal binding studies, might be expected to attract Cl^- to the interface, but there is no evidence of this from the TXRF measurements. Nevertheless, some daptomycin-Ca^{2+} must become bound to the PG/3adLPG [1:1] mix according to the monolayer adsorption data (Fig. S5), supporting the findings from vesicle binding studies. Consequently, a different mode of interaction can be assumed.

From the GIXOS measurements, after an initial increase in interfacial roughening and SLD of the lipid tails in DPPG/DP3adLPG [1:1] post injection, there is no further development of these changes compared to that observed for the DPPG/DP3adLPG [7:3] monolayer. This suggests that there is less daptomycin interaction for the equimolar PG/3adLPG [1:1] mixture. This is supported by the liposomal binding data. The decreased size of crystallites observed for PG/3adLPG [7:3] in GIXD experiments was absent in PG/3adLPG [1:1] monolayers, implying that the lipid ion pairs are disrupted to a lesser degree in the presence of daptomycin-Ca^{2+}, also an adsorption at the lipid headgroups with less tendency to incorporate in the acyl chain region may be assumed (Fig. 8). The shift to an equimolar PG/3adLPG ratio, therefore, appears to make the PG in the lipid bilayer less available for daptomycin interaction at sufficiently low Ca^{2+} concentrations, which suggests that sequestration of membrane PG into PG/LPG ion pairs could play some role in daptomycin resistance in staphylococci.

4.6. PG/LPG ion pairing probably acts in combination with other daptomycin resistance mechamisms

Our results build upon previous findings, which showed that under mild pH conditions, the presence of synthetic native LPG in DMPC/DMPG/DMLPG [2:1:1] liposomes showed a small decrease in daptomycin binding affinity compared with DMPC/DMPG [3:1] vesicles [43]. Our results differ in a number of important ways, firstly showing that daptomycin binding to model staphylococcal membranes can occur in the presence of the stable LPG analogue 3adLPG, secondly that post-binding structural changes can induce significant membrane perturbation and permeabilization and thirdly that PG/3adLPG ion pairing in equimolar mixtures significantly reduces daptomycin binding. In the absence of potential PG/LPG ion pairing, daptomycin was shown to exhibit a weak affinity for DMLPG, possibly via the free hydroxyl of its headgroup glycerol [43]. This may be in part due to the predominance of neutral zwitterionic LPG species at pH 7.4 [89], which would not exhibit any charge repulsion against daptomycin-Ca^{2+}. In the liposomal binding experiments carried out for this study 3adLPG would be significantly ionised at pH 5.5 [48]. The resultant PG/3adLPG ion pairing in equimolar mixtures significantly reduces daptomycin binding, compared to the daptomycin-susceptible PG/3adLPG [2:1] model.

In bacterial cells, ion pairing between native LPG and PG is promoted under the acidic conditions encountered at the outer leaflet of the cell membrane [46], which is the target site of daptomycin. If such PG/LPG ion pairing were to occur in localized regions of the membrane actively involved in cell wall synthesis [5], this may in part explain the observed link between *mprF* expression, increased LPG biosynthesis, and daptomycin resistance [27,90]. Any such protection afforded by localized increases in membrane LPG would of course rely on the integrity of PG/LPG ion pairs. Since this in turn is dependent upon local Ca^{2+} concentrations which would be increased by the presence of daptomycin-Ca^{2+}, additional resistance factors which reduce exposure of the membrane to daptomycin may play equally if not more important roles in daptomycin resistance. Thus, the range of measures deployed by daptomycin resistant strains of *S. aureus*, which include increased cell wall thickness [27] and teichoic acid D-alanylation [85], in addition to increased conversion of PG to LPG [24] and CL [25], most likely provide a synergistic protection against daptomycin. It has even been demonstrated that increased *mprF* expression alone can facilitate decreased susceptibility to daptomycin when decoupled from LPG synthesis via a putative efflux action of the MprF flopase subunit [31]. Considering the number of different observed daptomycin resistant phenotypes, it seems clear that LPG is unlikely to be solely responsible for increasing resistance to the antibiotic. Therefore, the combined effect of these different resistance mechanisms, including the sequestration of PG into PG/LPG ion pairs, may yet prove to be much more important than any individual factor.

5. Conclusions

In our model systems, the presence of 3adLPG in quantities less than equimolar with PG can promote lateral domain formation in monolayers or bilayers. In the presence of calcium ions, a PG/3adLPG [7:3] mixture likely consists of Ca^{2+} cross-linked PG/PG pairs and PG/3adLPG ion pairs. These phase-separated domains facilitate membrane interaction with daptomycin-Ca^{2+} through the displacement of Ca^{2+} from PG/PG pairs, giving access to the target lipid PG. The subsequent increase in local calcium concentration enables the displacement of 3adLPG from ion pairs with PG. This appears to create a kind of chain-reaction leading to increased daptomycin binding and decreasing PG/3adLPG domain size. In the leakage experiments with liposomes containing fully saturated DP3adLPG, this increased daptomycin binding seems sufficient to cause enhanced membrane permeability. Model systems made from equimolar PG/3adLPG mixtures show a marked reduction of

daptomycin binding, through full sequestration of the PG into ion pairs with 3adLPG, theoretically creating a single homogeneous phase. This does not render equimolar PG/3adLPG non-susceptible to daptomycin binding, because a sufficiently high local Ca^{2+} concentration facilitates displacement of the 3adLPG, making the PG available to daptomycin. Therefore, the key to the protective effect exerted by 3adLPG on reduced daptomycin-Ca^{2+}/PG binding lies in there being sufficient quantities of the LPG lipid analogue to sequester the available PG, and local Ca^{2+} concentrations being low enough not to split the PG/3adLPG ion pairs.

Supplementary information

Full descriptions of microbiological assays showing the effects of daptomycin membrane activity. Gibbs adsorption isotherm of daptomycin. All background-corrected TRXF spectra. Lipid monolayer GIXD diffraction patterns in the absence of subphase daptomycin and all Q_{xy} integrations showing the time-dependent effects of daptomycin adsorption to the monolayer-coated air/liquid interface. Tables summarizing Q_{xy} and Q_z integrated Bragg peak positions and the lipid 2D lattice parameters obtained from Bragg peak fitting. Representative examples of fits to the GIXOS data, together with tabulated layer thickness and scattering length density parameters obtained from GIXOS data fitting, showing the effects of daptomycin interfacial adsorption on monolayer structure. Additional leakage data.

CRediT authorship contribution statement

Maria Hoernke: Writing – review & editing, Writing – original draft, Visualization, Supervision, Project administration, Methodology, Investigation, Funding acquisition, Formal analysis, Data curation, Conceptualization. **Shuai Shi:** Visualization, Investigation, Formal analysis. **Alasdair T.M. Hubbard:** Methodology, Investigation, Formal analysis. **Nina Geringer:** Investigation. **Fabio Strati:** Investigation. **Chen Shen:** Writing – review & editing, Writing – original draft, Software, Methodology, Investigation, Formal analysis, Conceptualization. **Christian Wölk:** Writing – review & editing, Writing – original draft, Visualization, Methodology, Investigation, Formal analysis, Data curation, Conceptualization. **Richard D. Harvey:** Writing – review & editing, Writing – original draft, Visualization, Supervision, Project administration, Methodology, Investigation, Funding acquisition, Formal analysis, Data curation, Conceptualization.

Declaration of competing interest

The authors declare that they have no known competing financial interests or personal relationships that could have inappropriately influenced the work reported in this paper.

Acknowledgments

MH and SS gratefully acknowledge the Heerklotz lab at University of Freiburg for access to instrumentation and laboratory infrastructure. This work was funded by the German Research Foundation (DFG 415894560) to MH and SS. We also gratefully acknowledge DESY (Hamburg, Germany), a member of the Helmholtz Association HGF, for the awarding of beamtime to RDH and CW (I 11007433) and for provision of experimental facilities at PETRA III. We would also like to thank Dr. Florian Bertram for additional technical assistance on beamline P08.

Appendix A. Supplementary data

Supplementary data to this article can be found online at https://doi.org/10.1016/j.bbamem.2025.184452.

Data availability

The raw data supporting the conclusions made in this article will be supplied, upon reasonable request, by the corresponding authors.

References

[1] C.T.M. Mascio, J.D. Alder, J.A. Silverman, Bactericidal action of Daptomycin against stationary-phase and nondividing Staphylococcus aureus cells, Antimicrob. Agents Chemother. 51 (2007) 4255–4260, https://doi.org/10.1128/AAC.00824-07.
[2] J.H. Jorgensen, L.A. Maher, J.S. Redding, In vitro activity of LY146032 (Daptomycin) against selected aerobic bacteria, Eur. J. Clin. Microbiol. 6 (1987) 91–96, https://doi.org/10.1007/BF02097209.
[3] K.E. Piper, J.M. Steckelberg, R. Patel, R. Patel, In vitro activity of daptomycin against clinical isolates of Gram-positive bacteria, J. Infect. Chemother. 11 (2005) 207–209, https://doi.org/10.1007/s10156-005-0395-X.
[4] J.M. Streit, R.N. Jones, H.S. Sader, Daptomycin activity and spectrum: a worldwide sample of 6737 clinical Gram-positive organisms, J. Antimicrob. Chemother. 53 (2004) 669–674, https://doi.org/10.1093/jac/dkh143.
[5] F. Grein, A. Müller, K.M. Scherer, X. Liu, K.C. Ludwig, A. Klöckner, M. Strach, H. Sahl, U. Kubitscheck, T. Schneider, Ca2+-daptomycin targets cell wall biosynthesis by forming a tripartite complex with undecaprenyl-coupled intermediates and membrane lipids, Nat. Commun. 11 (2020) 1455, https://doi.org/10.1038/s41467-020-15257-1.
[6] J. Zhang, W.R.P. Scott, F. Gabel, M. Wu, R. Desmond, J.H. Bae, G. Zaccai, W. R. Algar, S.K. Straus, On the quest for the elusive mechanism of action of daptomycin: binding, fusion, and oligomerization, Biochimica et Biophysica Acta (BBA) 1865 (2017) 1490–1499, https://doi.org/10.1016/j.bbapap.2017.07.020.
[7] D. Beriashvili, R. Taylor, B. Kralt, N. Abu Mazen, S.D. Taylor, M. Palmer, Mechanistic studies on the effect of membrane lipid acyl chain composition on daptomycin pore formation, Chem. Phys. Lipids 216 (2018) 73–79, https://doi.org/10.1016/j.chemphyslip.2018.09.015.
[8] J.A. Buttress, A.-B. Schäfer, A. Koh, J. Wheatley, K. Mickiewicz, M. Wenzel, H. Strahl, The last resort antibiotic daptomycin exhibits two independent antibacterial mechanisms of axction, (n.d.). doi:https://doi.org/10.1101/2024.12.20.629673.
[9] M.-T. Lee, W.-C. Hung, M.-H. Hsieh, H. Chen, Y.-Y. Chang, H.W. Huang, Molecular state of the membrane-active antibiotic daptomycin, Biophys. J. 113 (2017) 82–90, https://doi.org/10.1016/j.bpj.2017.05.025.
[10] A. Pokorny, T.O. Khatib, H. Stevenson, A quantitative model of daptomycin binding to lipid bilayers, J. Phys. Chem. B 122 (2018) 9137–9146, https://doi.org/10.1021/acs.jpcb.8b07503.
[11] R. Taylor, K. Butt, B. Scott, T. Zhang, J.K. Muraih, E. Mintzer, S. Taylor, M. Palmer, Two successive calcium-dependent transitions mediate membrane binding and oligomerization of daptomycin and the related antibiotic A54145, Biochimica et Biophysica Acta (BBA) 1858 (2016) 1999–2005, https://doi.org/10.1016/j.bbamem.2016.05.020.
[12] A.-B. Hachmann, E.R. Angert, J.D. Helmann, Genetic analysis of factors affecting susceptibility of Bacillus subtilis to daptomycin, Antimicrob. Agents Chemother. 53 (2009) 1598–1609, https://doi.org/10.1128/AAC.01329-08.
[13] S.D. Taylor, M. Palmer, The action mechanism of daptomycin, Bioorganic Med. Chem. 24 (2016) 6253–6268, https://doi.org/10.1016/j.bmc.2016.05.052.
[14] R. Moreira, S.D. Taylor, Establishing the structure-activity relationship between phosphatidylglycerol and daptomycin, ACS Infect. Dis. 8 (2022) 1674–1686, https://doi.org/10.1021/acsinfecdis.2c00262.
[15] A. Howe, S. Sofou, Daptomycin-induced lipid phases on model lipid bilayers: effect of lipid type and of lipid leaflet order on membrane permeability, J. Phys. Chem. B 125 (2021) 5775–5785, https://doi.org/10.1021/acs.jpcb.1c02047.
[16] R. Moreira, S.D. Taylor, The chiral target of Daptomycin is the 2 R,2′ S stereoisomer of phosphatidylglycerol, Angew. Chemie. 134 (2022), https://doi.org/10.1002/ange.202114858.
[17] M.A. Kreutzberger, A. Pokorny, P.F. Almeida, Daptomycin–Phosphatidylglycerol domains in lipid membranes, Langmuir 33 (2017) 13669–13679, https://doi.org/10.1021/ACS.LANGMUIR.7B01841/SUPPL_FILE/LA7B01841_SI_002.PDF.
[18] A. Müller, M. Wenzel, H. Strahl, F. Grein, T.N.V. Saaki, B. Kohl, T. Siersma, J. E. Bandow, H.-G. Sahl, T. Schneider, Daptomycin inhibits cell envelope synthesis by interfering with fluid membrane microdomains, Proc. Natl. Acad. Sci. 113 (2016) E7077–E7086.
[19] D.A. Gray, M. Wenzel, More than a pore: a current perspective on the in vivo mode of action of the lipopeptide antibiotic daptomycin, Antibiotics 9 (2020) 17, https://doi.org/10.3390/antibiotics9010017.
[20] L. Cui, E. Tominaga, H.-m. Neoh, K. Hiramatsu, Correlation between reduced daptomycin susceptibility and vancomycin resistance in vancomycin-intermediate *Staphylococcus aureus*, Antimicrob. Agents Chemother. 50 (2006) 1079–1082, https://doi.org/10.1128/AAC.50.3.1079-1082.2006.
[21] J.A. Silverman, N. Oliver, T. Andrew, L.I. Tongchuan, Resistance studies with daptomycin, Antimicrob. Agents Chemother. 45 (2001) 1799–1802, https://doi.org/10.1128/AAC.45.6.1799-1802.2001.
[22] H.E. Hasper, N.E. Kramer, J.L. Smith, J.D. Hillman, C. Zachariah, O.P. Kuipers, B. De Kruijff, E. Breukink, An alternative bactericidal mechanism of action for lantibiotic peptides that target lipid II, Science 80 (313) (2006) 1636–1637, https://doi.org/10.1126/science.1129818.
[23] N.N. Mishra, A.S. Bayer, C. Weidenmaier, T. Grau, S. Wanner, A. Stefani, V. Cafiso, T. Bertuccio, M.R. Yeaman, C.C. Nast, S.-J.J. Yang, S. Stefani, V. Cafiso,

T. Bertuccio, M.R. Yeaman, C.C. Nast, S.-J.J. Yang, Phenotypic and genotypic characterization of daptomycin-resistant methicillin-resistant *Staphylococcus aureus* strains: relative roles of *mprF* and *dlt* operons, PLoS One 9 (2014) e107426, https://doi.org/10.1371/journal.pone.0107426.

[24] A.S. Bayer, N.N. Mishra, A.L. Cheung, A. Rubio, S.-J. Yang, Dysregulation of mprF and dltABCD expression among daptomycin-non-susceptible MRSA clinical isolates, J. Antimicrob. Chemother. 71 (2016) 2100–2104.

[25] J.H. Jiang, M.S. Bhuiyan, H.H. Shen, D.R. Cameron, T.W.T. Rupasinghe, C.M. Wu, A.P. Le Brun, X. Kostoulias, C. Domene, A.J. Fulcher, M.J. McConville, B. P. Howden, G.J. Lieschke, A.Y. Peleg, Antibiotic resistance and host immune evasion in Staphylococcus aureus mediated by a metabolic adaptation, Proc. Natl. Acad. Sci. U. S. A. 116 (2019) 3722–3727, https://doi.org/10.1073/pnas.1812066116.

[26] T. Zhang, J.K. Muraih, B. MacCormick, J. Silverman, M. Palmer, Daptomycin forms cation- and size-selective pores in model membranes, Biochimica et Biophysica Acta (BBA) 1838 (2014) 2425–2430, https://doi.org/10.1016/j.bbamem.2014.05.014.

[27] N.N. Mishra, S.-J. Yang, A. Sawa, A. Rubio, C.C. Nast, M.R. Yeaman, A.S. Bayer, Analysis of cell membrane characteristics of in vitro-selected daptomycin-resistant strains of methicillin-resistant Staphylococcus aureus, Antimicrob. Agents Chemother. 53 (2009) 2312–2318, https://doi.org/10.1128/AAC.01682-08.

[28] A.Y. Peleg, S. Miyakis, D.V. Ward, A.M. Earl, A. Rubio, D.R. Cameron, S. Pillai, R. C. Moellering, G.M. Eliopoulos, Whole genome characterization of the mechanisms of daptomycin resistance in clinical and laboratory derived isolates of staphylococcus aureus, PloS One 7 (2012) e28316, https://doi.org/10.1371/journal.pone.0028316.

[29] R.P. Rehal, H. Marbach, A.T.M. Hubbard, A.A. Sacranie, F. Sebastiani, G. Fragneto, R.D. Harvey, The influence of mild acidity on lysyl-phosphatidylglycerol biosynthesis and lipid membrane physico-chemical properties in methicillin-resistant Staphylococcus aureus, Chem. Phys. Lipids 206 (2017) 60–70, https://doi.org/10.1016/j.chemphyslip.2017.06.007.

[30] T. Jones, M.R. Yeaman, G. Sakoulas, S.-J. Yang, R.A. Proctor, H.-G. Sahl, J. Schrenzel, Y.Q. Xiong, A.S. Bayer, Failures in clinical treatment of Staphylococcus aureus infection with daptomycin are associated with alterations in surface charge, membrane phospholipid asymmetry, and drug binding, Antimicrob. Agents Chemother. 52 (2008) 269–278, https://doi.org/10.1128/AAC.00719-07.

[31] C.M. Ernst, C.J. Slavetinsky, S. Kuhn, J.N. Hauser, M. Nega, N.N. Mishra, C. Gekeler, A.S. Bayer, A. Peschel, Gain-of-function mutations in the phospholipid Flippase MprF confer specific Daptomycin resistance, MBio 9 (2018), https://doi.org/10.1128/mBio.01659-18 e01659-18.

[32] J.F. Tocanne, P.H.J. Ververgaert, A.J. Verkleij, L.L.M. Van Deenen, A monolayer and freeze-etching study of charged phospholipids II. ionic properties of mixtures of phosphatidylglycerol and lysylphosphatidylglycerol, Chem. Phys. Lipids 12 (1974) 220–231.

[33] R.J. Smith, Calcium and Bacteria, Adv. Microb. Physiol. 37 (1995) 83–133, https://doi.org/10.1016/S0065-2911(08)60144-7.

[34] E.J. Findlay, P.G. Barton, Phase behavior of synthetic phosphatidylglycerols and binary mixtures with phosphatidylcholines in the presence and absence of calcium ions, Biochemistry 17 (1978) 2400–2405, https://doi.org/10.1021/bi00605a023.

[35] R.N.A.H. Lewis, R.N. McElhaney, The physicochemical properties of cardiolipin bilayers and cardiolipin-containing lipid membranes, Biochim. Biophys. Acta - Biomembr. 1788 (2009) 2069–2079, https://doi.org/10.1016/j.bbamem.2009.03.014.

[36] M. Sturm, O. Gutowski, G. Brezesinski, The influence of calcium traces in ultrapure water on the lateral organization in tetramyristoyl cardiolipin monolayers, ChemPhysChem 20 (2019) 1521–1526, https://doi.org/10.1002/cphc.201900126.

[37] S. Danner, G. Pabst, K. Lohner, A. Hickel, Structure and thermotropic behavior of the Staphylococcus aureus lipid lysyl-dipalmitoylphosphatidylglycerol, Biophys. J. 94 (2008) 2150–2159, https://doi.org/10.1529/biophysj.107.123422.

[38] P.I. Campbell, *Staphylococcus aureus* lysylphosphatidylglycerol: an unsuitable adjunct for preparing cationic liposomes, Microbios Lett. 19 (1982) 11–16.

[39] A.S. Bayer, N.N. Mishra, L. Chen, B.N. Kreiswirth, A. Rubio, S.J. Yang, Frequency and distribution of single-nucleotide polymorphisms within mprF in methicillin-resistant Staphylococcus aureus clinical isolates and their role in cross-resistance to daptomycin and host defense antimicrobial peptides, Antimicrob. Agents Chemother. 59 (2015) 4930–4937, https://doi.org/10.1128/AAC.00970-15.

[40] K.-M. Kang, N.N. Mishra, K.T. Park, G.-Y. Lee, Y.H. Park, A.S. Bayer, S.-J. Yang, Phenotypic and genotypic correlates of daptomycin-resistant methicillin-susceptible Staphylococcus aureus clinical isolates, J. Microbiol. 55 (2017) 153–159, https://doi.org/10.1007/s12275-017-6509-1.

[41] E. Kilelee, A. Pokorny, M.R. Yeaman, A.S. Bayer, Lysyl-Phosphatidylglycerol attenuates membrane perturbation rather than surface Association of the Cationic Antimicrobial Peptide 6W-RP-1 in a model membrane system: implications for Daptomycin resistance, Antimicrob. Agents Chemother. 54 (2010) 4476–4479, https://doi.org/10.1128/AAC.00191-10.

[42] T.O. Khatib, H. Stevenson, M.R. Yeaman, A.S. Bayer, A. Pokorny, Binding of Daptomycin to anionic lipid vesicles is reduced in the presence of Lysyl-Phosphatidylglycerol, Antimicrob. Agents Chemother. 60 (2016) 5051–5053, https://doi.org/10.1128/AAC.00744-16.

[43] R. Moreira, S.D. Taylor, The impact of lysyl-phosphatidylglycerol on the interaction of daptomycin with model membranes, Org. Biomol. Chem. 20 (2022) 9319–9329, https://doi.org/10.1039/d2ob01384c.

[44] E. Cox, A. Michalak, S. Pagentine, P. Seaton, A. Pokorny, Lysylated phospholipids stabilize models of bacterial lipid bilayers and protect against antimicrobial peptides, Biochim. Biophys. Acta (BBA)-Biomembranes. 1838 (2014) 2198–2204.

[45] R. Rehal, P.R.J. Gaffney, A.T.M. Hubbard, R.D. Barker, R.D. Harvey, The pH-dependence of lipid-mediated antimicrobial peptide resistance in a model staphylococcal plasma membrane: a two-for-one mechanism of epithelial defence circumvention, Eur. J. Pharm. Sci. 128 (2019) 43–53, https://doi.org/10.1016/j.ejps.2018.11.017.

[46] S.H. Collins, W.A. Hamilton, Magnitude of the protonmotive force in respiring Staphylococcus aureus and Escherichia coli, J. Bacteriol. 126 (1976) 1224–1231.

[47] C.M. Ernst, P. Staubitz, N.N. Mishra, S.-J. Yang, G. Hornig, H. Kalbacher, A. S. Bayer, D. Kraus, A. Peschel, The bacterial Defensin resistance protein MprF consists of separable domains for lipid Lysinylation and antimicrobial peptide repulsion, PLoS Pathog. 5 (2009) e1000660, https://doi.org/10.1371/journal.ppat.1000660.

[48] C. Wölk, H. Youssef, T. Guttenberg, H. Marbach, G. Vizcay-Barrena, C. Shen, G. Brezesinski, R.D. Harvey, Phase diagram for a Lysyl-phosphatidylglycerol analogue in biomimetic mixed monolayers with Phosphatidylglycerol: insights into the tunable properties of bacterial membranes, Chemphyschem (2020) cphc.202000026, https://doi.org/10.1002/cphc.202000026.

[49] C. Shen, R. Kirchhof, F. Bertram, A grazing incidence diffraction setup for Langmuir trough experiments at the high-resolution diffraction beamline P08 at PETRA III, J. Phys. Conf. Ser. 2380 (2022), https://doi.org/10.1088/1742-6596/2380/1/012047.

[50] O.H. Seeck, C. Deiter, K. Pflaum, F. Bertram, A. Beerlink, H. Franz, J. Horbach, H. Schulte-Schrepping, B.M. Murphy, M. Greve, O. Magnussen, The high-resolution diffraction beamline P08 at PETRA III, J. Synchrotron Radiat. 19 (2012) 30–38, https://doi.org/10.1107/S0909049511047236.

[51] J. Als-Nielsen, D. Jacquemain, K. Kjaer, F. Leveiller, M. Lahav, L. Leiserowitz, Principles and applications of grazing incidence X-ray and neutron scattering from ordered molecular monolayers at the air-water interface, Phys. Rep. 246 (1994) 251–313, https://doi.org/10.1016/0370-1573(94)90046-9.

[52] D. Jacquemain, S.G. Wolf, F. Leveiller, M. Deutsch, K. Kjaer, J. Als-Nielsen, M. Lahav, L. Leiserowitz, Two-dimensional crystallography of amphiphilic molecules at the air–water interface, Angew. Chemie Int. Ed. English. 31 (1992) 130–152, https://doi.org/10.1002/anie.199201301.

[53] V.M. Kaganer, H. Möhwald, P. Dutta, Structure and phase transitions in Langmuir monolayers, Rev. Mod. Phys. 71 (1999) 779–819, https://doi.org/10.1103/revmodphys.71.779.

[54] C. Stefaniu, G. Brezesinski, X-ray investigation of monolayers formed at the soft air/water interface, Curr. Opin. Colloid Interface Sci. 19 (2014) 216–227, https://doi.org/10.1016/j.cocis.2014.01.004.

[55] K. Kjaer, Some simple ideas on X-ray reflection and grazing-incidence diffraction from thin surfactant films, Physica B: Condensed Matter 198 (1994) 100–109, https://doi.org/10.1016/0921-4526(94)90137-6.

[56] C. Stefaniu, C. Wölk, G. Brezesinski, E. Schneck, Relationship between structure and molecular interactions in monolayers of specially designed aminolipids, Nanoscale Adv. 1 (2019) 3529–3536, https://doi.org/10.1039/c9na00355j.

[57] R. Ziblat, L. Leiserowitz, L. Addadi, Crystalline lipid domains: characterization by X-ray diffraction and their relation to biology, Angew. Chemie - Int. Ed. 50 (2011) 3620–3629, https://doi.org/10.1002/anie.201004470.

[58] L. Wiegart, B. Struth, Geometric boundary condition for the chain alignment in lipid monolayers, Phys. B Condens. Matter (2005) 126–129, https://doi.org/10.1016/j.physb.2004.11.040.

[59] C. Stefaniu, V.M. Latza, O. Gutowski, P. Fontaine, G. Brezesinski, E. Schneck, Headgroup-ordered monolayers of uncharged glycolipids exhibit selective interactions with ions, J. Phys. Chem. Lett. 10 (2019) 1684–1690, https://doi.org/10.1021/acs.jpclett.8b03865.

[60] M. Sturm, O. Gutowski, G. Brezesinski, The effect of pH on the structure and lateral organization of cardiolipin in Langmuir monolayers, ChemPhysChem 23 (2022), https://doi.org/10.1002/cphc.202200218.

[61] T. Schoonjans, A. Brunetti, B. Golosio, M. Sanchez Del Rio, V.A. Solé, C. Ferrero, L. Vincze, The xraylib library for X-ray-matter interactions. Recent developments, Spectrochim. Acta - part B, At. Spectrosc. 66 (2011) 776–784, https://doi.org/10.1016/j.sab.2011.09.011.

[62] Y. Dai, B. Lin, M. Meron, K. Kim, B. Leahy, O.G. Shpyrko, A comparative study of Langmuir surfactant films: grazing incidence x-ray off-specular scattering vs. x-ray specular reflectivity, J. Appl. Phys. 110 (2011) 102213, https://doi.org/10.1063/1.3661980.

[63] L. Wiegart, B. Struth, M. Tolan, P. Terech, Thermodynamic and structural properties of phospholipid Langmuir monolayers on hydrosol surfaces, Langmuir 21 (2005) 7349–7357, https://doi.org/10.1021/la050478m.

[64] J. Pusterla, E. Scoppola, C. Appel, T. Mukhina, C. Shen, G. Brezesinski, E. Schneck, Characterization of lipid bilayers adsorbed to functionalized air/water interfaces, Nanoscale 14 (2022) 15048–15059, https://doi.org/10.1039/d2nr03334h.

[65] C. Shen, H. Zhang, B.M. Ocko, Reconstructing the reflectivity of liquid surfaces from grazing incidence X-ray off-specular scattering data, J. Appl. Cryst. 57 (2024) 714–727, https://doi.org/10.1107/S1600576724002887.

[66] J.H. Lakey, M. Ptak, Fluorescence indicates a calcium-dependent interaction between the lipopeptide antibiotic LY 146032 and phospholipid membranes, Biochemistry 27 (1988) 4639–4645, https://doi.org/10.1021/bi00413a009.

[67] H. Patel, C. Tscheka, H. Heerklotz, Characterizing vesicle leakage by fluorescence lifetime measurements, Soft Matter 5 (2009) 2849, https://doi.org/10.1039/b908524f.

[68] S. Shi, H. Fan, M. Hoernke, Leaky membrane fusion: an ambivalent effect induced by antimicrobial polycations, Nanoscale Adv. 4 (2022) 5109–5122, https://doi.org/10.1039/D2NA00464J.

[69] G.R. Bartlett, Phosphorus assay in column chromatography, J. Biol. Chem. 234 (1959) 466–468, https://doi.org/10.1111/j.1365-2621.1976.tb01121.x.

[70] G. Brezesinski, E. Schneck, Investigating ions at amphiphilic monolayers with X-ray fluorescence, Langmuir 35 (2019) 8531–8542, https://doi.org/10.1021/acs.langmuir.9b00191.
[71] P.M. Macdonald, J. Seelig, Calcium binding to mixed phosphatidylglycerol-phosphatidylcholine bilayers as studied by deuterium nuclear magnetic resonance, Biochemistry 26 (1987) 6292–6298, https://doi.org/10.1021/bi00379a005.
[72] C. Ege, M.K. Ratajczak, J. Majewski, K. Kjaer, K.Y.C. Lee, Evidence for lipid/cholesterol ordering in model lipid membranes, Biophys. J. 91 (2006), https://doi.org/10.1529/biophysj.106.085134.
[73] J. Als-Nielsen, K. Kjær, X-Ray Reflectivity and Diffraction Studies of Liquid Surfaces and Surfactant Monolayers, Springer, Boston, MA, 1989, pp. 113–138, https://doi.org/10.1007/978-1-4613-0551-4_11.
[74] K. Beck, J. Nandy, M. Hoernke, Membrane permeabilization can be crucially biased by a fusogenic lipid composition – leaky fusion caused by antimicrobial peptides in model membranes, Soft Matter 19 (2023) 2919–2931, https://doi.org/10.1039/D2SM01691E.
[75] D. Jung, A. Rozek, M. Okon, R.E.W. Hancock, Structural transitions as determinants of the action of the calcium-dependent antibiotic daptomycin, Chem. Biol. 11 (2004) 949–957, https://doi.org/10.1016/j.chembiol.2004.04.020.
[76] A. Stulz, A. Vogt, J.S. Saar, L. Akil, K. Lienkamp, M. Hoernke, Quantified membrane Permeabilization indicates the lipid selectivity of membrane-active antimicrobials, Langmuir 35 (2019) 16366–16376, https://doi.org/10.1021/acs.langmuir.9b01849.
[77] S. Shi, N. Quarta, H. Zhang, Z. Lu, M. Hof, R. Šachl, R. Liu, M. Hoernke, Hidden complexity in membrane permeabilization behavior of antimicrobial polycations, Phys. Chem. Chem. Phys. 23 (2021) 1475–1488, https://doi.org/10.1039/d0cp05651k.
[78] S. Shi, A.M. Markl, Z. Lu, R. Liu, M. Hoernke, Interplay of fusion, leakage, and electrostatic lipid clustering: membrane perturbations by a hydrophobic antimicrobial polycation, Langmuir 38 (2022) 2379–2391, https://doi.org/10.1021/acs.langmuir.1c03445.
[79] A.-V. Villar, A. Alonso, F.M. Goñi, Articles Leaky Vesicle Fusion Induced by Phosphatidylinositol-Specific Phospholipase C: Observation of Mixing of Vesicular Inner Monolayers †, 2000, https://doi.org/10.1021/bi992515c.
[80] S.T. Yang, E. Zaitseva, L.V. Chernomordik, K. Melikov, Cell-penetrating peptide induces leaky fusion of liposomes containing late endosome-specific anionic lipid, Biophys. J. 99 (2010) 2525–2533, https://doi.org/10.1016/j.bpj.2010.08.029.
[81] W.C. Wimley, K. Hristova, The mechanism of membrane Permeabilization by peptides: still an enigma, Aust. J. Chem. 73 (2020) 96–103, https://doi.org/10.1071/CH19449.
[82] J.K. Muraih, J. Harris, S.D. Taylor, M. Palmer, Characterization of daptomycin oligomerization with perylene excimer fluorescence: stoichiometric binding of phosphatidylglycerol triggers oligomer formation, Biochimica et Biophysica Acta (BBA) 1818 (2012) 673–678, https://doi.org/10.1016/j.bbamem.2011.10.027.
[83] R. Rehal, R.D. Barker, Z. Lu, T.T. Bui, B. Demé, G. Hause, C. Wölk, R.D. Harvey, Lipid domain formation and non-lamellar structures associated with varied lysylphosphatidylglycerol analogue content in a model staphylococcal plasma membrane, Biochim. Biophys. Acta Biomembr. 1863 (2021) 183571, https://doi.org/10.1016/J.BBAMEM.2021.183571.
[84] R.H. Baltz, Daptomycin: mechanisms of action and resistance, and biosynthetic engineering, Curr. Opin. Chem. Biol. 13 (2009) 144–151, https://doi.org/10.1016/j.cbpa.2009.02.031.
[85] Z. Ma, E. Lasek-Nesselquist, J. Lu, R. Schneider, R. Shah, G. Oliva, J. Pata, K. McDonough, M.P. Pai, W.E. Rose, Characterization of genetic changes associated with daptomycin nonsusceptibility in Staphylococcus aureus, PloS One 13 (2018) e0198366.
[86] A.T. Duran, H. Marbach, B. Rasul, K.L. Andrew Chan, R.D. Harvey, Fourier transform infrared spectroscopy detection of lipid ion-pairing in the *Staphylococcus aureus* plasma membrane, FASEB J. 30 (2016) 877.1.
[87] P. Garidel, A. Blume, 1,2-Dimyristoyl-sn-glycero-3-phosphoglycerol (DMPG) monolayers: influence of temperature, pH, ionic strength and binding of alkaline earth cations, Chem. Phys. Lipids 138 (2005) 50–59, https://doi.org/10.1016/j.chemphyslip.2005.08.001.
[88] S.D. Shoemaker, T.K. Vanderlick, Calcium modulates the mechanical properties of anionic phospholipid membranes, J. Colloid Interface Sci. 266 (2003) 314–321, https://doi.org/10.1016/S0021-9797(03)00582-4.
[89] J.F. Tocanne, P.H.J.T. Ververgaert, A.J. Verkleij, L.L.M. van Deenen, A monolayer and freeze-etching study of charged phospholipids I. Effects of ions and pH on the ionic properties of phosphatidylglycerol and lysylphosphatidylglycerol, Chem. Phys. Lipids 12 (1974) 201–219, https://doi.org/10.1016/0009-3084(74)90075-9.
[90] N.N. Mishra, A.S. Bayer, Correlation of cell membrane lipid profiles with daptomycin resistance in methicillin-resistant staphylococcus aureus, Antimicrob. Agents Chemother. 57 (2013) 1082–1085, https://doi.org/10.1128/AAC.02182-12.